### 6.3.3.3 44 BWR Uncanistered Fuel Waste Package

A two-dimensional finite-element thermal model of the large 44 BWR UCF WP conceptual design was developed by the M&O Waste Package Design Group. Model detail including the separate layers of the basket tube design for each disposal container design is provided with the figures in Appendix B. Intimate contact was assumed between the layers of stainless steel and aluminum, and also between the tube guides and inner shell. The UCF WP fill gas was assumed to be helium. The analysis is described in detail in a supporting design analysis (CRWMS M&O 1995q).

The finite-element code ANSYS was used to model the two-dimensional cross-section of the UCF WP. Time and position-dependent temperatures for the WP surface were exported from the emplacement model, described in Section 6.2.1.1.1, and applied as time-varying boundary conditions. The other time-varying conditions used in the model were the design basis SNF decay heat outputs applied as volumetric heat generations to the assembly areas of the model and use smeared material properties. The effective conductivity for the assembly area for a PWR assembly was developed as described in Section 6.2.1.2. For the purpose of the BWR thermal evaluation, it was assumed that the effective conductivity developed for a PWR assembly can be applied to the peak cladding temperature determination for a BWR assembly. It is expected that the effective conductivity for a BWR will be higher; therefore, slightly conservative temperatures will be predicted using the PWR effective conductivity. The heat loads for the assembly areas were interpolated from the Oak Ridge database of SNF characteristics for the assumed thermal design basis SNF. The heat load will decrease logarithmically with time as the fission products decay. The heat loads were applied volumetrically and were multiplied by an axial heat peaking factor to approximate the axial center of the WP with a two-dimensional model. An SNF assembly is much hotter at the mid-length than at the ends, and it is conservative to assume the two-dimensional WP model represents the hottest cross-section of the UCF WP.

The boundary conditions and heat loads were applied and solved out to 1,000 years for each of the five thermal loading scenarios described in Section 6.2.1.1.1 with the MGDS BWR thermal design basis SNF type described in Table 6.3-1. Table 6.3-4 summarizes the peak temperatures and the time of occurrence for each of the cases analyzed. The thermal loading scenarios indicated in Table 6.3-4 are defined in Table 6.3-1, and the thermal design basis SNF description is provided in Table 6.2-1. Both "conservative" estimates of peak cladding temperatures using the Wooton-Epstein correlation and "best estimate" predictions using the effective conductivity method are presented in the table. Peak cladding temperatures using effective conductivity are calculated directly in the ANSYS program, and Wooton-Epstein calculations for each time step in the ANSYS analysis were also performed for comparison.

Table 6.3-4. 44 BWR Uncanistered Fuel Waste Package Thermal Analysis Results

| Thermal Load | Design Basis SNF | Peak Cladding | | | | Peak Basket | | WP Surface | |
|---|---|---|---|---|---|---|---|---|---|
| | | Conservative Estimate | | Best Estimate | | | | | |
| | | °C | yrs | °C | yrs | °C | yrs | °C | yrs |
| High #1 | MGDS | 285 | 5 | 270 | 8 | 265 | 8 | 188 | 50 |
| High #2 | MGDS | 277 | 4 | 261 | 5 | 256 | 5 | 165 | 40 |
| Low #1 | MGDS | 267 | 0.8 | 249 | 0.9 | 242 | 1 | 117 | 8 |
| Low #2 | MGDS | 272 | 2 | 254 | 2 | 248 | 2 | 131 | 8 |
| Low #3 | MGDS | 280 | 2 | 263 | 2 | 257 | 3 | 146 | 10 |

Figure 6.3-20 displays the thermal history of the 44 BWR UCF WP at 83 MTU/acre (20.5 kgU/m$^2$) for the MGDS thermal design basis SNF. Figure 6.3-21 displays the temperature profile across the UCF basket and disposal container for the time of peak internal temperatures (five years). The peak estimate for high thermal loading #2 SNF cladding temperature was 261°C, which can be compared to the estimate of 277°C that was calculated with the Wooton-Epstein correlation. Both SNF cladding temperature estimates are comfortably below the cladding temperature limit of 350°C. Just as for the 21 PWR UCF WP, peak temperatures occur between the time of emplacement and the time of peak drift wall temperatures.

Figure 6.3-22 displays the temperature contours in the 44 BWR UCF WP at the time of peak temperatures, five years. The thermal loading for this case was 83 MTU/acre (20.5 kgU/m$^2$) and the MGDS thermal design basis SNF was assumed. Figures 6.3-23, 6.3-24, and 6.3-25 display the temperature contours for the same case at 10, 50, and 100 years, respectively. By 100 years, the temperature drop across the WP (from center to edge) has dropped to less than 35°C.

Figure 6.3-26 displays the thermal history of the 44 BWR UCF WP at 100 MTU/acre (24.7 kgU/m$^2$) for the MGDS design basis SNF. This combination of a short WP spacing and high thermal loading resulted in the highest temperatures of all of the cases considered and represents an upper bound of possible thermal loadings. SNF cladding temperatures peaked at 270°C (285°C using Wooton-Epstein) and average repository horizon temperatures remained above 150°C for hundreds of years. Just as for the 21 PWR UCF WP cases, above-boiling, near-field temperatures persisted past 1,000 years.

Figures 6.3-27 and 6.3-28 display the thermal history of the 44 BWR UCF WP at 25 MTU/acre (6.2 kgU/m$^2$) with the MGDS design basis SNF for low thermal load #1 and low thermal load #2, respectively. Peak internal temperatures are similar to those for the high thermal loading because the peaks occur before any effects of thermal loading have been realized. However, as thermal loading effects emerge, all of the low thermal loading results converge, as described in Section 6.2.1.1.1. Figure 6.3-29 displays the thermal history of the 44 BWR UCF WP for low thermal load #3 with the MGDS thermal design basis SNF. The highest internal temperature occurred where the MGDS thermal design basis SNF and the shortest WP spacing (16.2 m) defines the thermal loading. The peak temperatures occur before drift-to-drift effects emerge such that the

WP spacing drives the peak near-field temperatures and high thermal load #1 and low thermal load #3 have nearly the same peak cladding temperatures.

The thermal evaluation of the 44 BWR UCF WP conceptual design with respect to the repository has considered a number of thermal loading scenarios. The repository thermal loading has not been specified and will not be finally established for years. Therefore, the WP thermal behavior has been analyzed for a range of thermal loadings. For each repository thermal loading scenario, a three-dimensional repository emplacement and two-dimensional WP evaluation were performed. The results of the thermal evaluations indicate that the 44 BWR UCF WP design satisfies the thermal limitations for disposal in the MGDS.

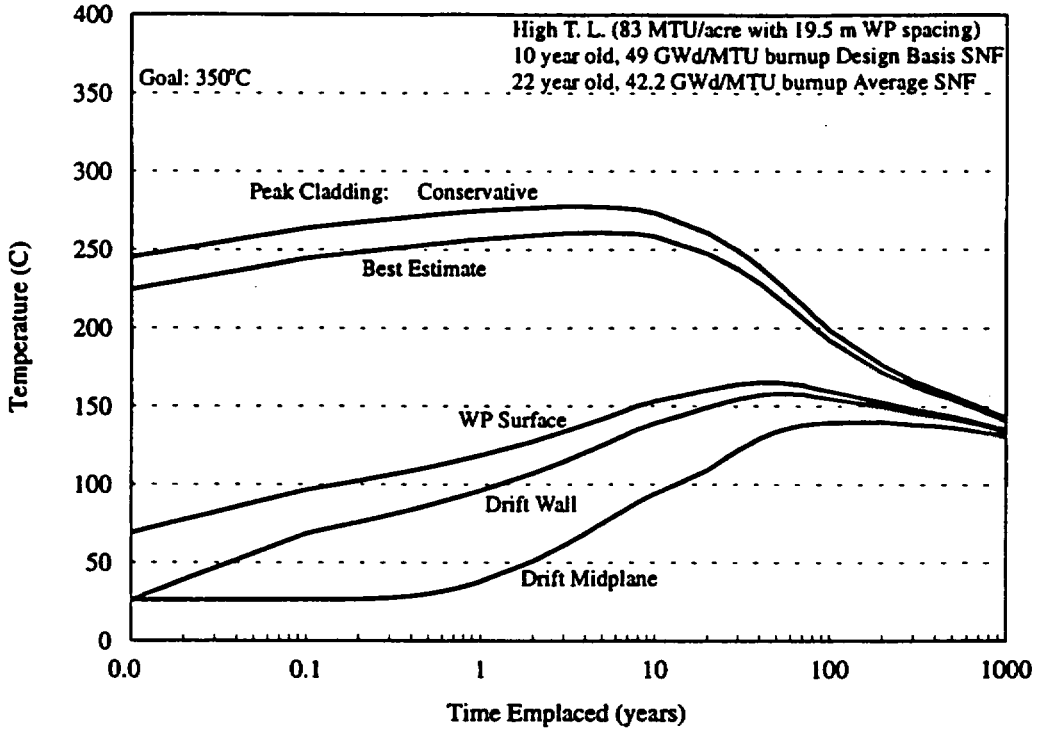


Figure 6.3-20. 44 BWR UCF, High Thermal Load (#2), MGDS DBF

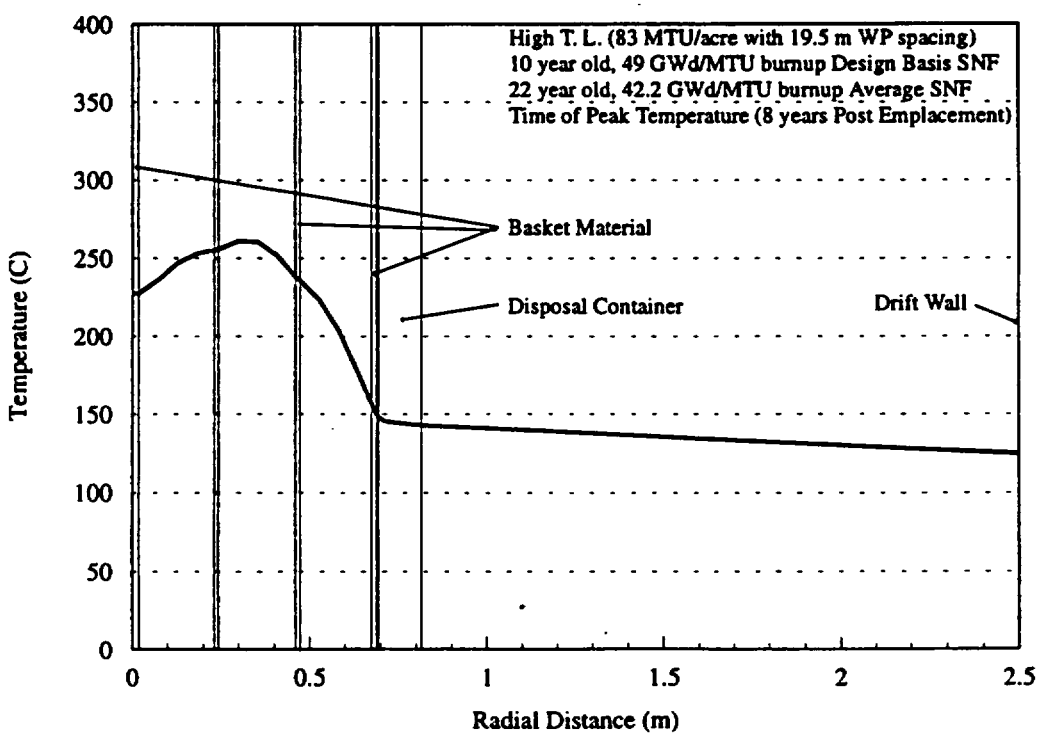


Figure 6.3-21. Temperature Profile, 44 BWR UCF, 45° Angle Through Peak Temperature

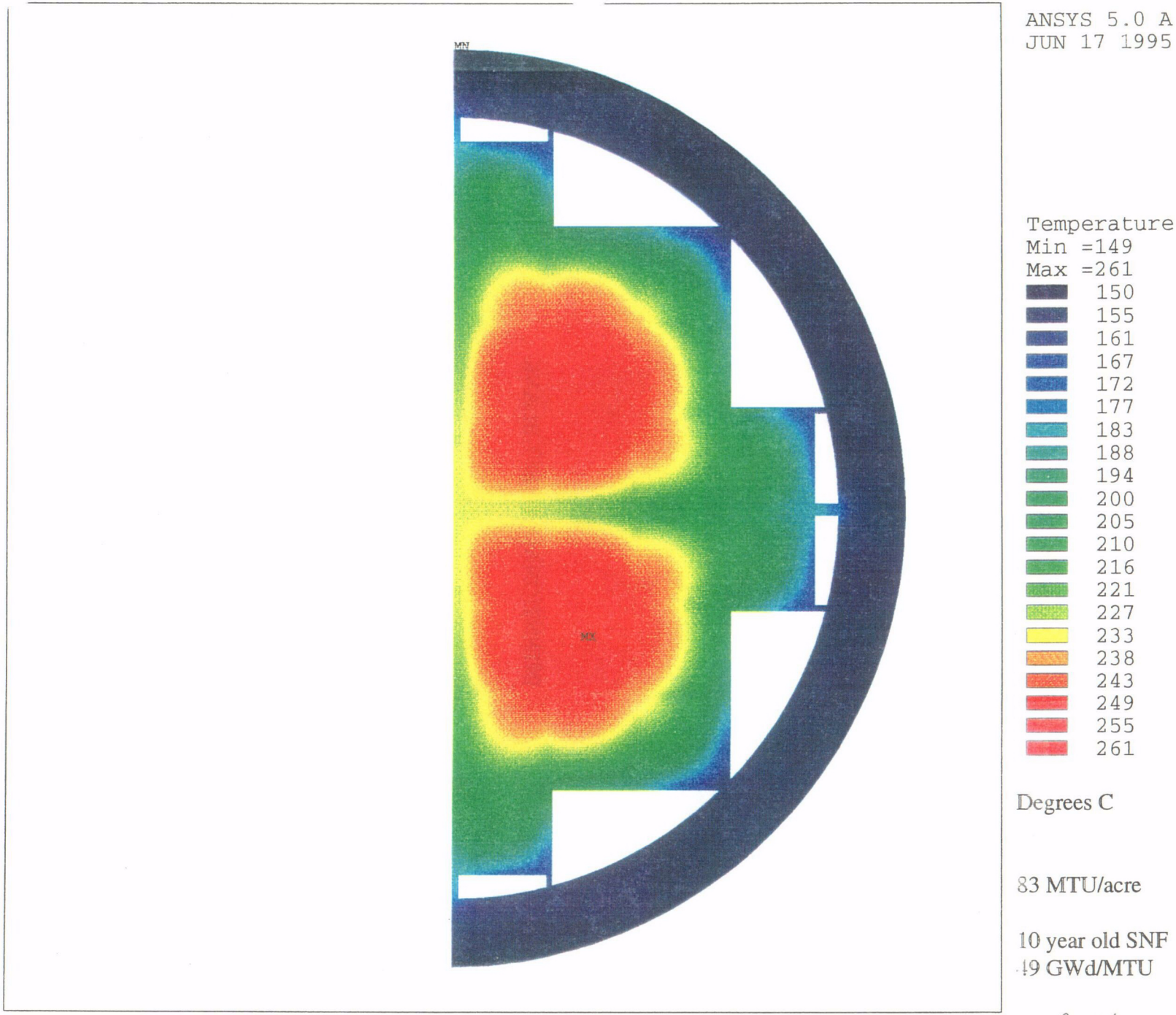


Figure 6.3-22. 44 BWR UCF Peak Temperatures (5 Years)

C01

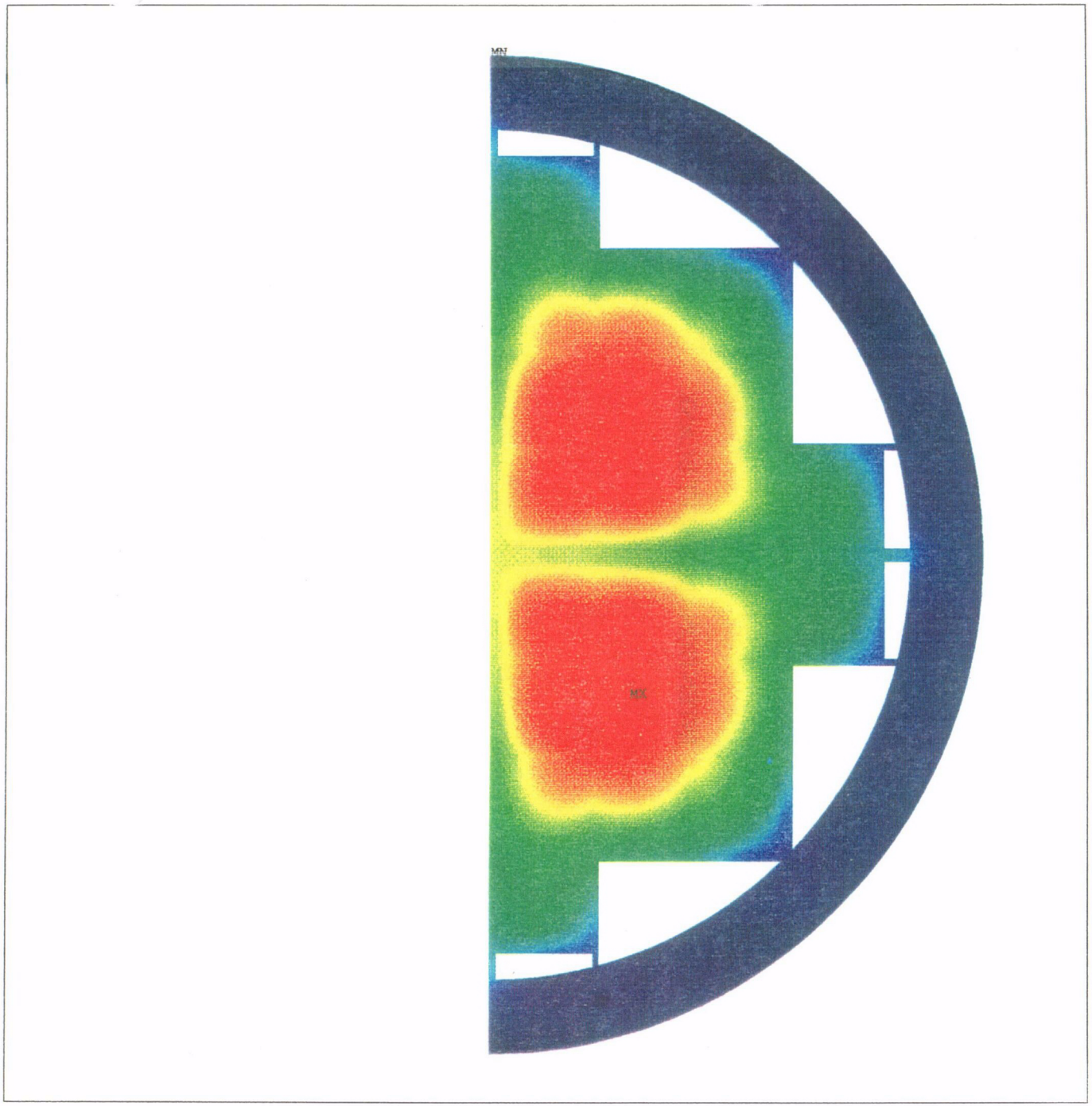


Figure 6.3-23. 44 BWR UCF Temperatures at 10 Years

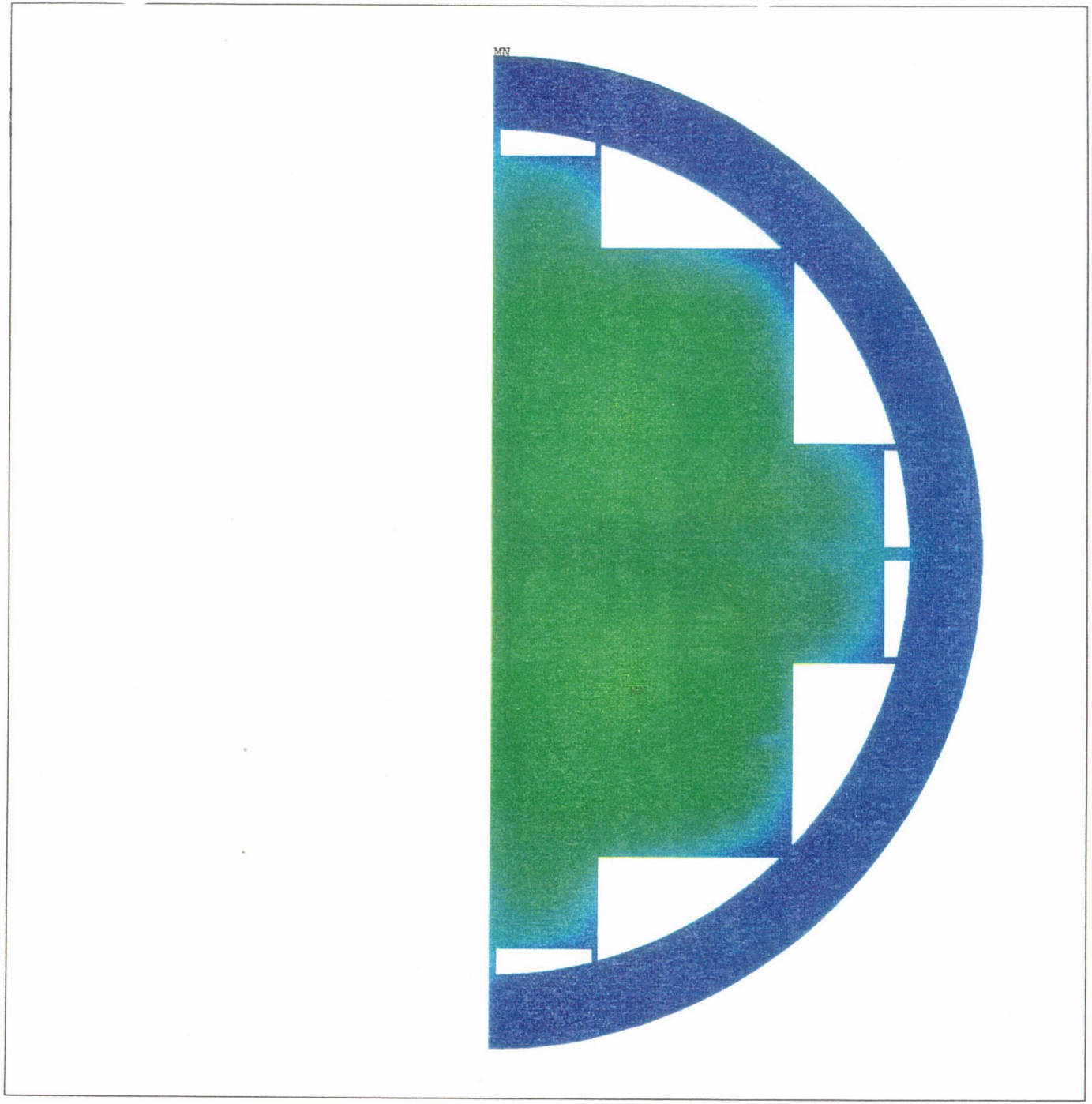


C03

Figure 6.3-24. 44 BWR UCF Temperatures at 50 Years

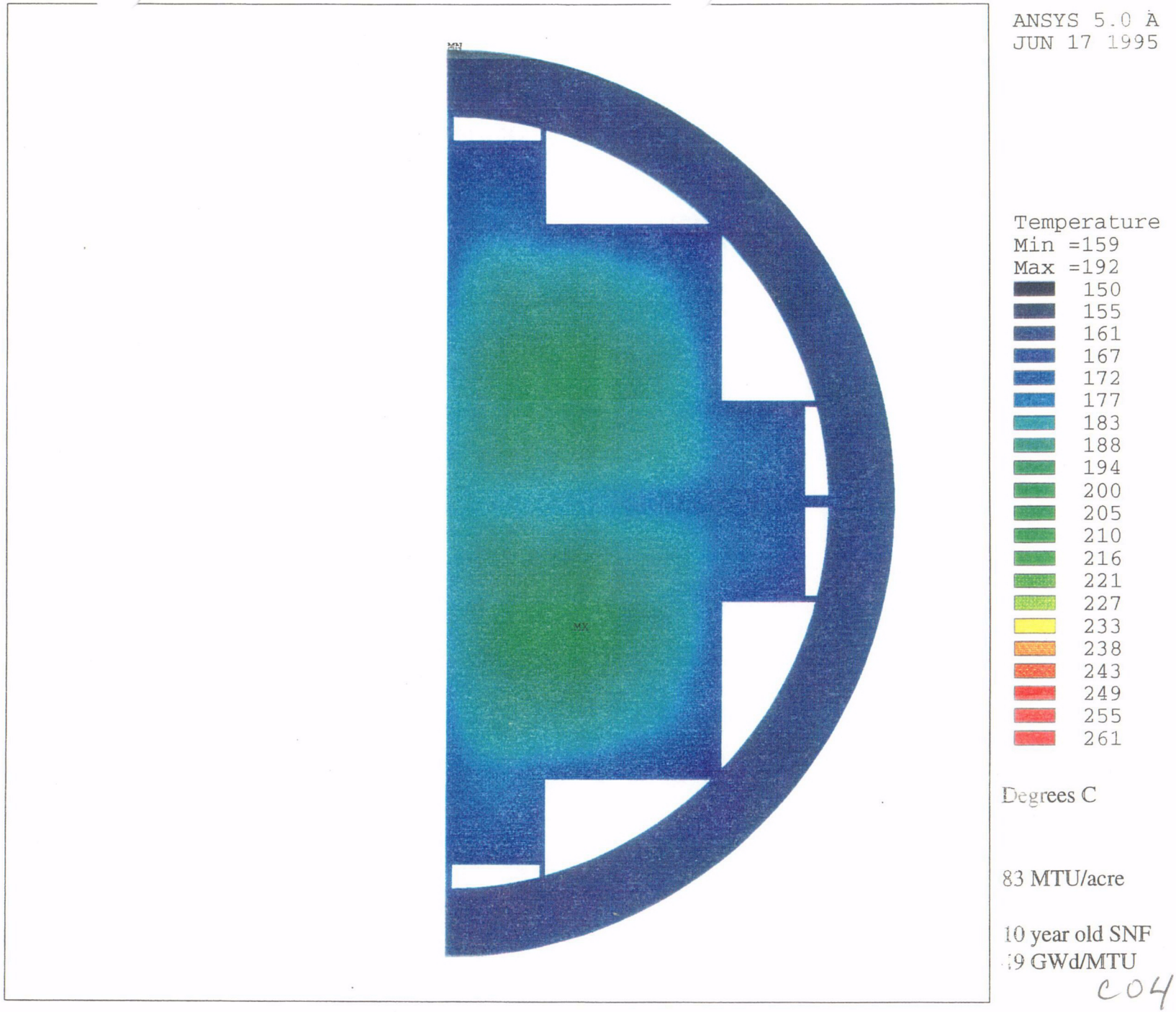


Figure 6.3-25. 44 BWR UCF Temperatures at 100 Years

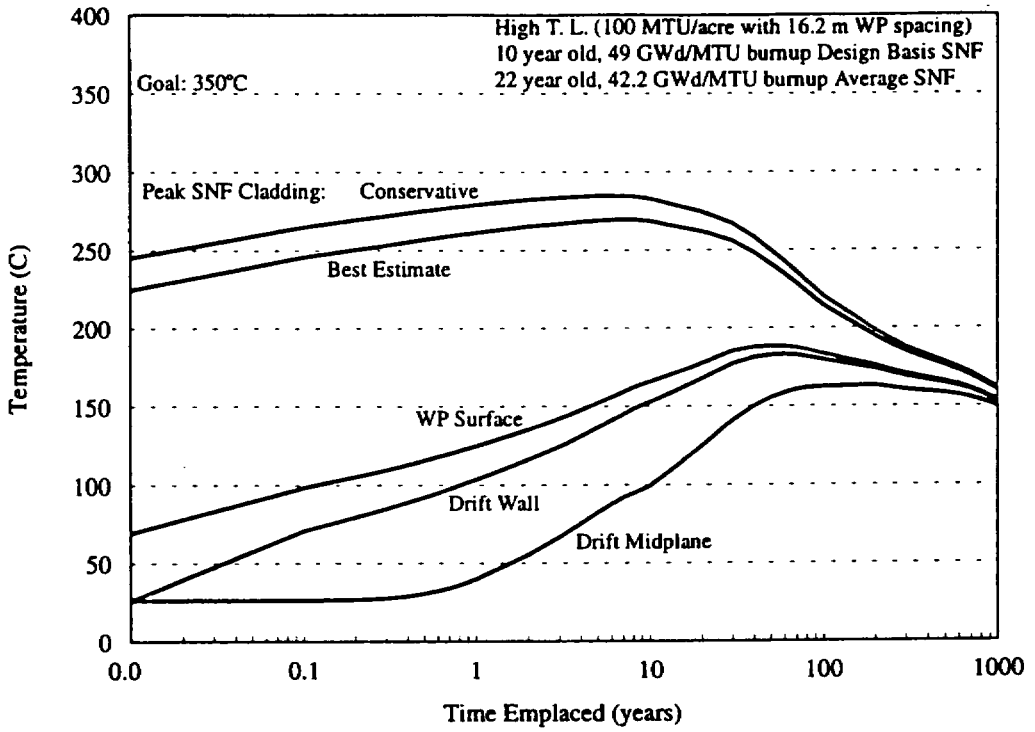


Figure 6.3-26. 44 BWR UCF, High Thermal Load (#1), MGDS DBF

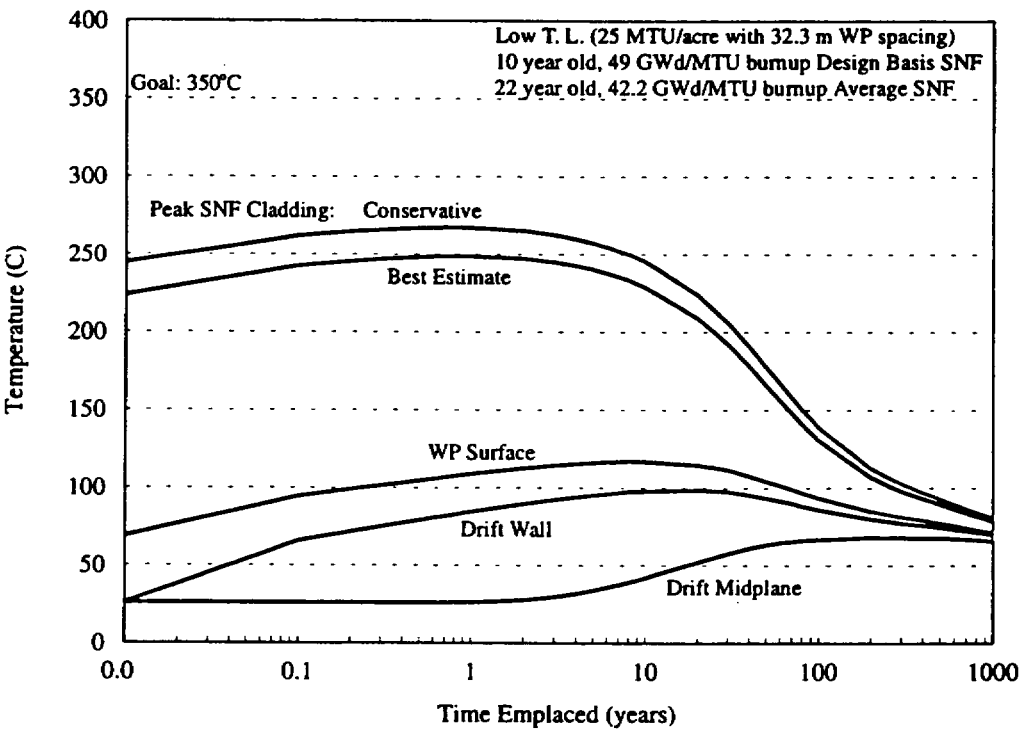


Figure 6.3-27. 44 BWR UCF, Low Thermal Load (#1), MGDS DBF

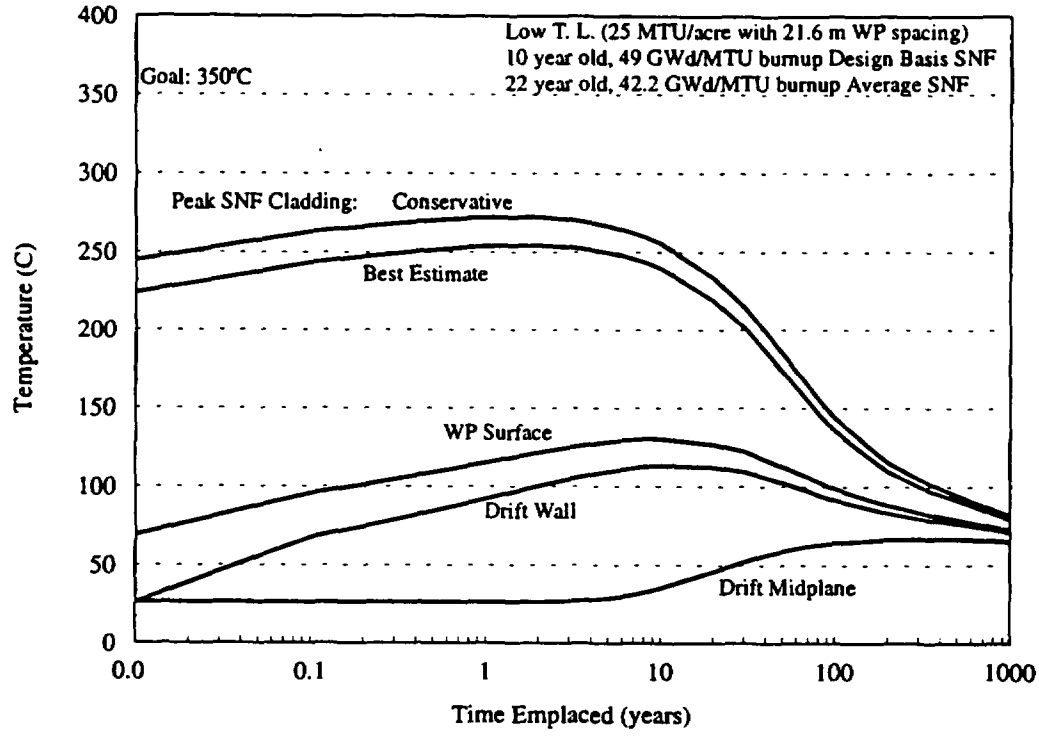


Figure 6.3-28. 44 BWR UCF, Low Thermal Load (#2), MGDS DBF

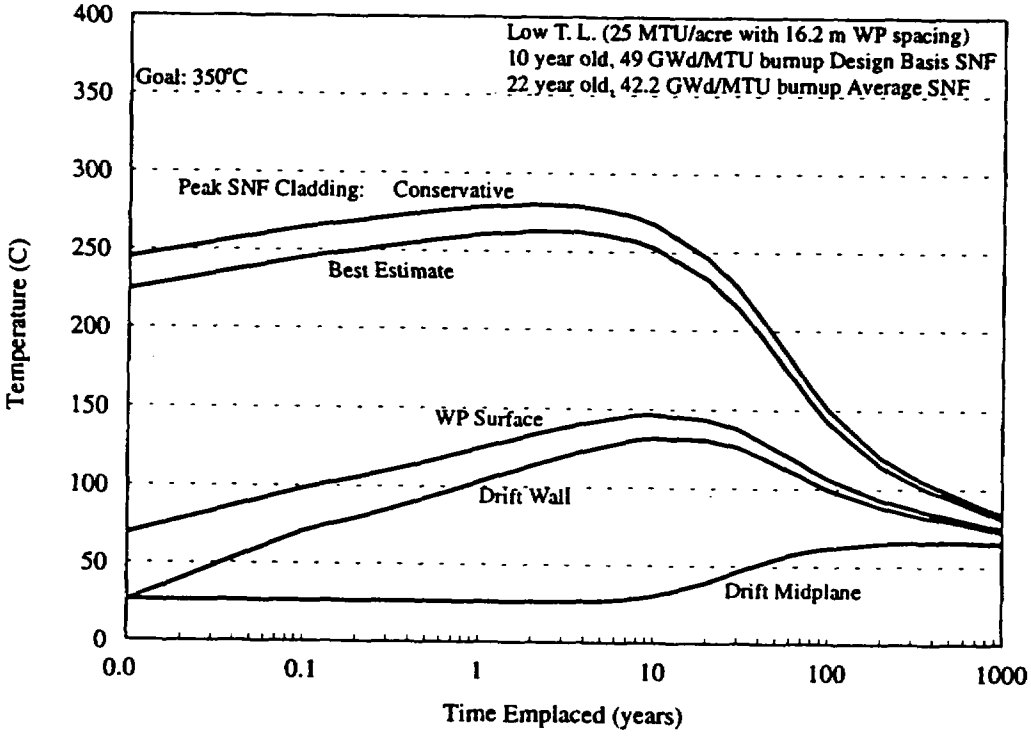


Figure 6.3-29. 44 BWR UCF, Low Thermal Load (#3), MGDS DBF

### 6.3.3.4 24 BWR Uncanistered Fuel Waste Package

A two-dimensional finite-element thermal model of the small 24 BWR UCF WP conceptual design was developed by the M&O Waste Package Design Group. Model detail including the separate layers of the basket tube design for each disposal container design is provided with the figures in Appendix B. Intimate contact was assumed between the layers of stainless steel and aluminum, and also between the tube guides and inner shell. The UCF WP fill gas was assumed to be helium. The analysis is described in detail in a supporting design analysis (CRWMS M&O 1995r).

The finite-element code ANSYS was used to model the two-dimensional cross-section of the UCF WP. Time and position-dependent temperatures for the WP surface were exported from the emplacement model, described in Section 6.2.1.1.2, and applied as time-varying boundary conditions. The other time-varying conditions used in the model were the design basis SNF decay heat outputs applied as volumetric heat generations to the assembly areas of the model and use smeared material properties. Similar to the 44 BWR UCF WP analysis, the effective conductivity for the assembly area was assumed to be same as described in Section 6.2.1.2 for PWR assemblies. It is expected that the effective conductivity for a BWR will be higher; therefore, slightly conservative temperatures will be predicted using the PWR effective conductivity. The heat loads for the assembly areas were interpolated from the Oak Ridge database of SNF characteristics for each of the assumed design basis SNF. The heat load will decrease logarithmically with time as the fission products decay. The heat loads were applied volumetrically and were multiplied by an axial heat peaking factor to approximate the axial center of the WP with a two-dimensional model. An SNF assembly is much hotter at the mid-length than at the ends, and it is conservative to assume the two-dimensional WP model represents the hottest cross-section of the UCF WP.

The boundary conditions and heat loads were applied and solved out to 1,000 years for each of the five thermal loading scenarios described in Section 6.2.1.1.2 with the MGDS BWR thermal design basis SNF described in Table 6.3-1. Table 6.3-5 summarizes the peak temperatures and the time of occurrence for each of the cases analyzed. The thermal loading scenarios indicated in Table 6.3-5 are defined in Table 6.2-2, and the thermal design basis SNF description is provided in Table 6.3-1. Both "conservative" estimates of peak cladding temperatures using the Wooton-Epstein correlation, and "best estimate" predictions using the effective conductivity method are presented in the table. Peak cladding temperatures using effective conductivity are calculated directly in the ANSYS program, and Wooton-Epstein calculations for each time step in the ANSYS analysis were also performed for comparison.

Figure 6.3-30 displays the thermal history of the 24 BWR UCF WP at 83 MTU/acre (20.5 kgU/m$^2$) for the MGDS thermal design basis SNF. Figure 6.3-31 displays the temperature profile across the UCF basket and disposal container for the time of peak internal temperatures (10 years). The peak estimate for high thermal loading #2 SNF cladding temperature was 211°C, which can be compared to the estimate of 230°C that was calculated with the Wooton-Epstein correlation. Both SNF cladding temperature estimates are comfortably below the cladding temperature limit of 350°C. Just as for the 21 PWR UCF WP, peak temperatures occur between the time of emplacement and the time of peak drift wall temperatures.

Table 6.3-5. 24 BWR UCF WP Thermal Analysis Results

| Thermal Load | Design Basis SNF | Peak Cladding | | | | Peak Basket | | WP Surface | |
|---|---|---|---|---|---|---|---|---|---|
| | | Conservative Estimate | | Best Estimate | | | | | |
| | | °C | yrs | °C | yrs | °C | yrs | °C | yrs |
| High #1 | MGDS | 242 | 10 | 225 | 20 | 222 | 30 | 184 | 60 |
| High #2 | MGDS | 230 | 8 | 211 | 10 | 207 | 10 | 160 | 50 |
| Low #1 | MGDS | 208 | 1 | 183 | 2 | 177 | 2 | 101 | 20 |
| Low #2 | MGDS | 218 | 3 | 195 | 3 | 190 | 4 | 118 | 10 |
| Low #3 | MGDS | 230 | 4 | 209 | 5 | 204 | 4 | 137 | 10 |

Figure 6.3-32 displays the temperature contours in the 24 BWR UCF WP at the time of peak temperatures, 10 years. The thermal loading was 83 MTU/acre (20.5 kgU/m$^2$) and the MGDS thermal design basis SNF was assumed. Figures 6.3-33 and 6.3-34 display the temperature contours for the same case at 50 and 100 years, respectively. By 100 years, the temperature drop across the WP (from center to edge) has dropped to less than 25°C.

Figure 6.3-35 displays the thermal history of the 24 BWR UCF WP at 100 MTU/acre (24.7 kgU/m$^2$) for the MGDS design basis SNF. This combination of a short WP spacing and high thermal loading resulted in the highest temperatures of all of the cases considered and represents an upper bound of possible thermal loadings. SNF cladding temperatures peaked at 225°C (242°C using Wooton-Epstein) and average repository horizon temperatures remained above 150°C for hundreds of years. Just as for the 21 PWR UCF WP cases, above-boiling, near-field temperatures persisted past 1,000 years.

Figures 6.3-36 and 6.3-37 display the thermal history of the 24 BWR UCF WP at 25 MTU/acre (6.2 kgU/m$^2$) with the MGDS design basis SNF for low thermal load #1 and low thermal load #2, respectively. Peak internal temperatures are similar to those for the high thermal loading because the peaks occur before any effects of thermal loading have been realized. However, as thermal loading effects emerge, all of the low thermal loading results converge as described in Section 6.2.1.1.2. Figure 6.3-38 displays the thermal history of the 24 BWR UCF WP for low thermal load #3 with the MGDS thermal design basis SNF.

The highest internal temperature occurred where the MGDS thermal design basis SNF and the shortest WP spacing (16.2 m) defines the thermal loading. The peak temperatures occur before drift-to-drift effects emerge such that the WP spacing drives the peak near-field temperatures and high thermal load #1 and low thermal load #3 have nearly the same peak cladding temperatures.

The thermal evaluation of the 24 BWR UCF WP conceptual design with respect to the repository has considered a number of thermal loading scenarios. The repository thermal loading has not been specified and will not be finally established for years. Therefore, the WP thermal behavior has been analyzed for a range of thermal loadings. For each repository thermal loading scenario, a three-dimensional repository emplacement and two-dimensional WP evaluation were performed. The results of the thermal evaluations indicate that the 24 BWR UCF WP design satisfies the thermal limitations for disposal in the MGDS.

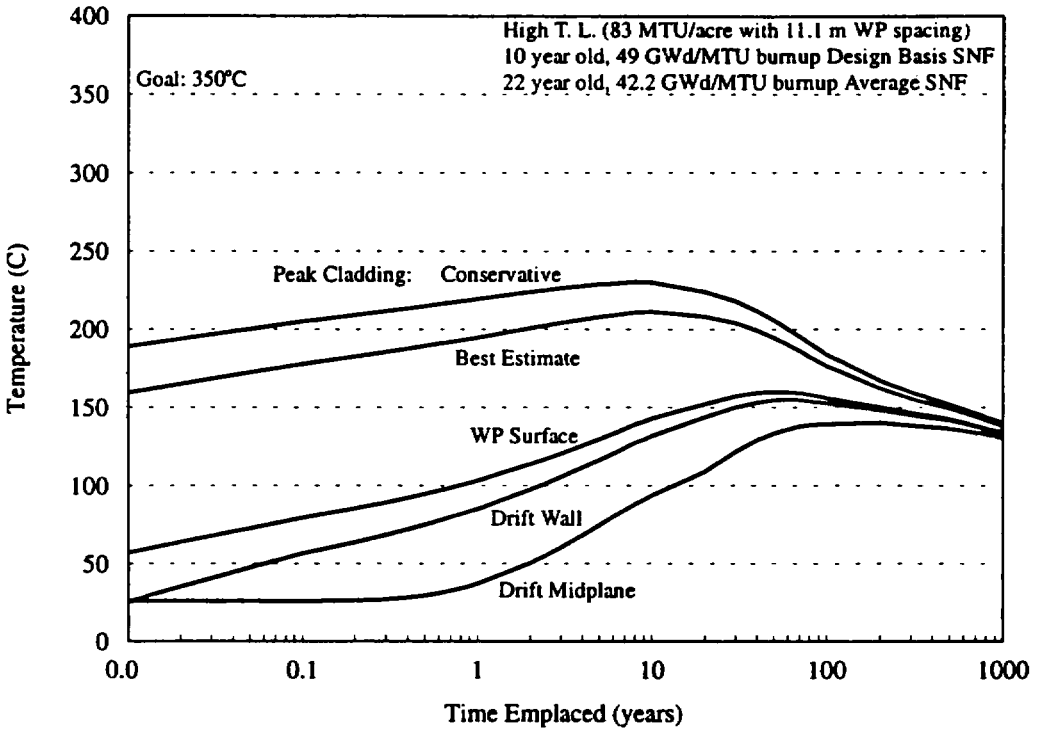


Figure 6.3-30. 24 BWR UCF, High Thermal Load (#2), MGDS DBF

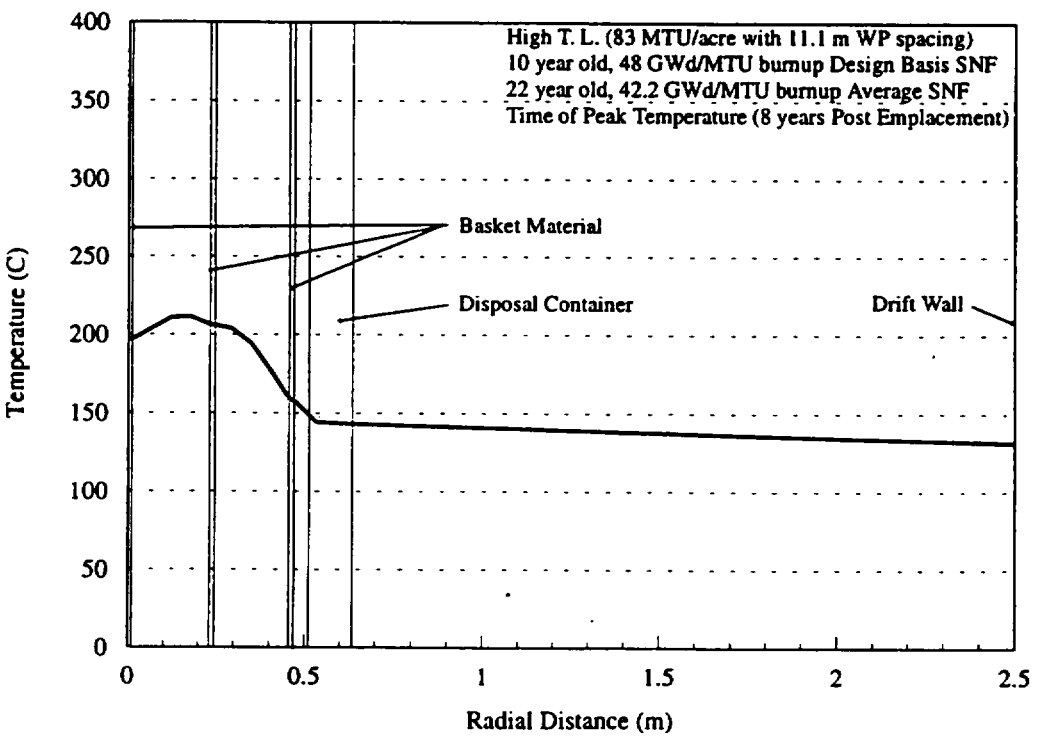


Figure 6.3-31. Temperature Profile, 24 BWR UCF, 45° Angle Through Peak Temperatures

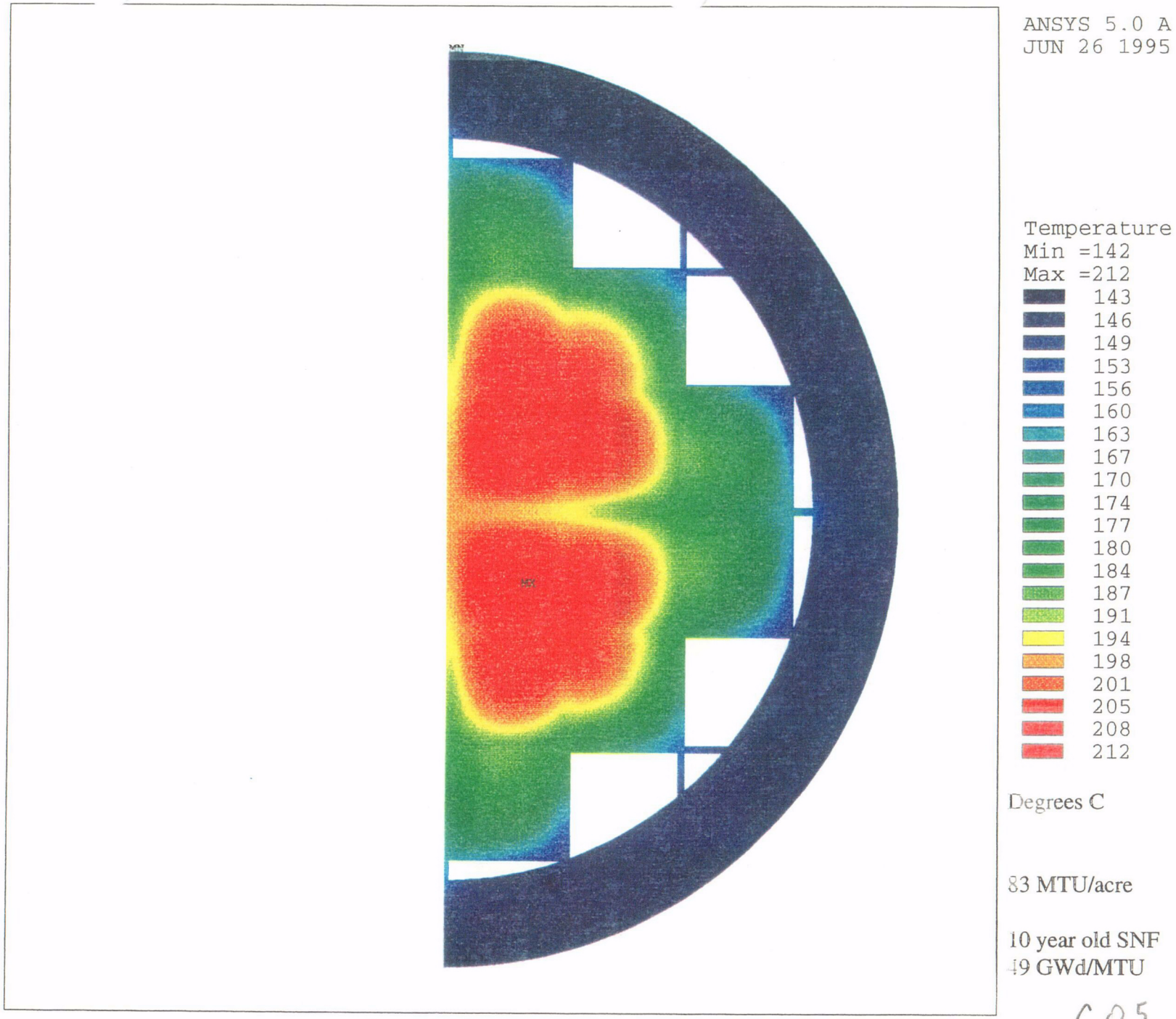


C05

Figure 6.3-32. 24 BWR UCF Peak Temperatures (10 Years)

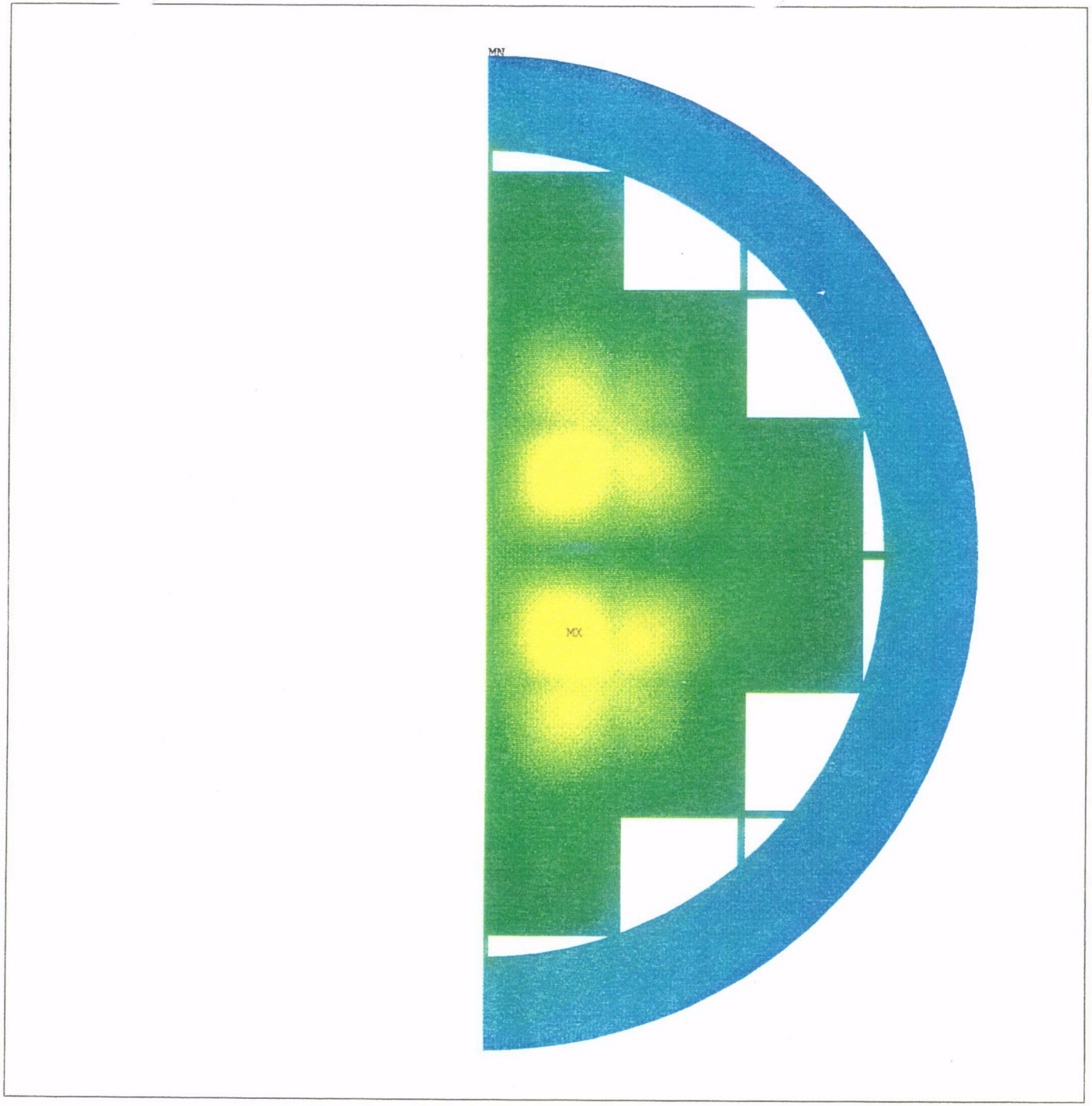


Figure 6.3-33. 24 BWR UCF Temperatures at 50 Years

C06

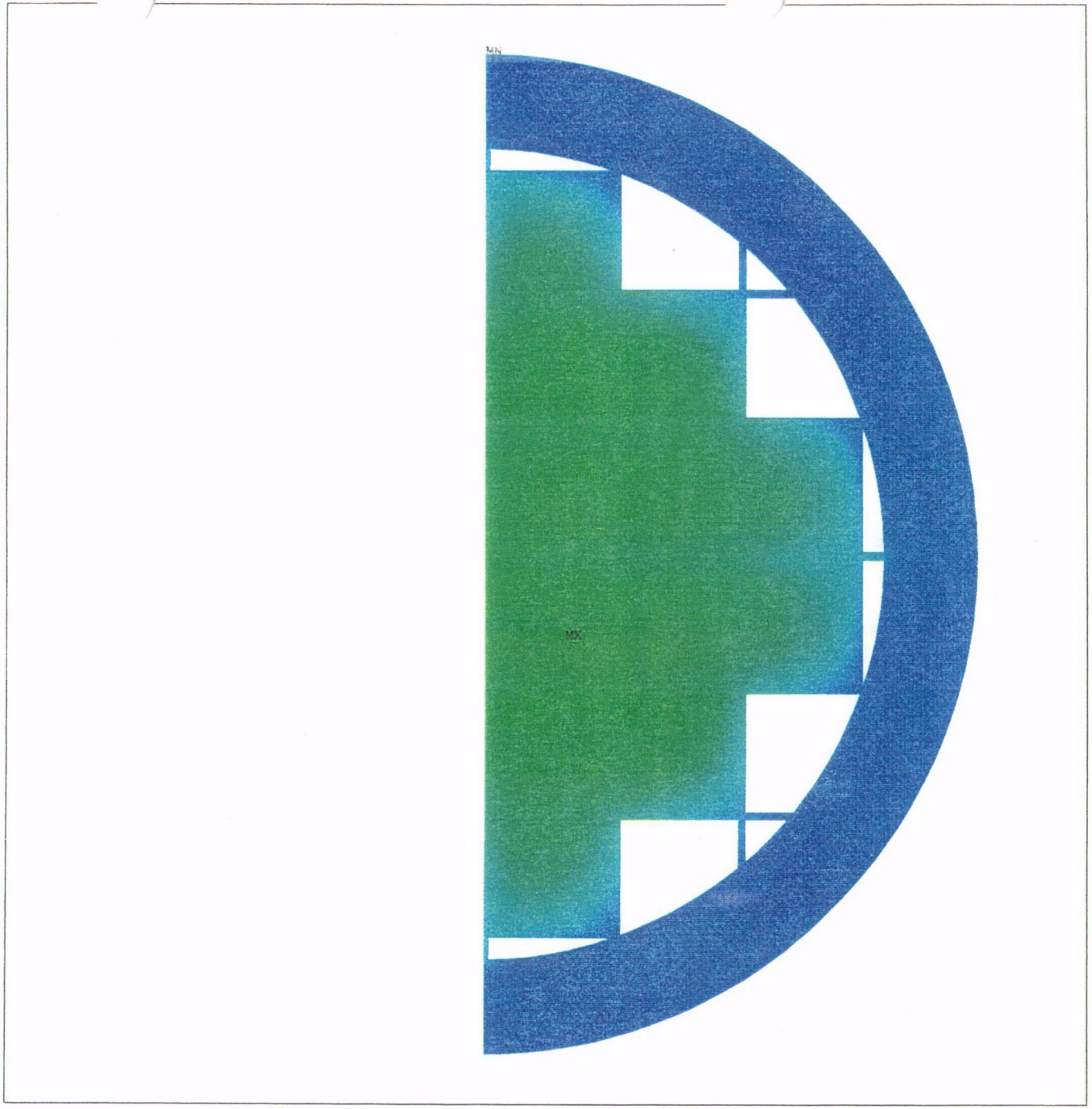


Figure 6.3-34. 24 BWR MPC Temperatures at 100 Years

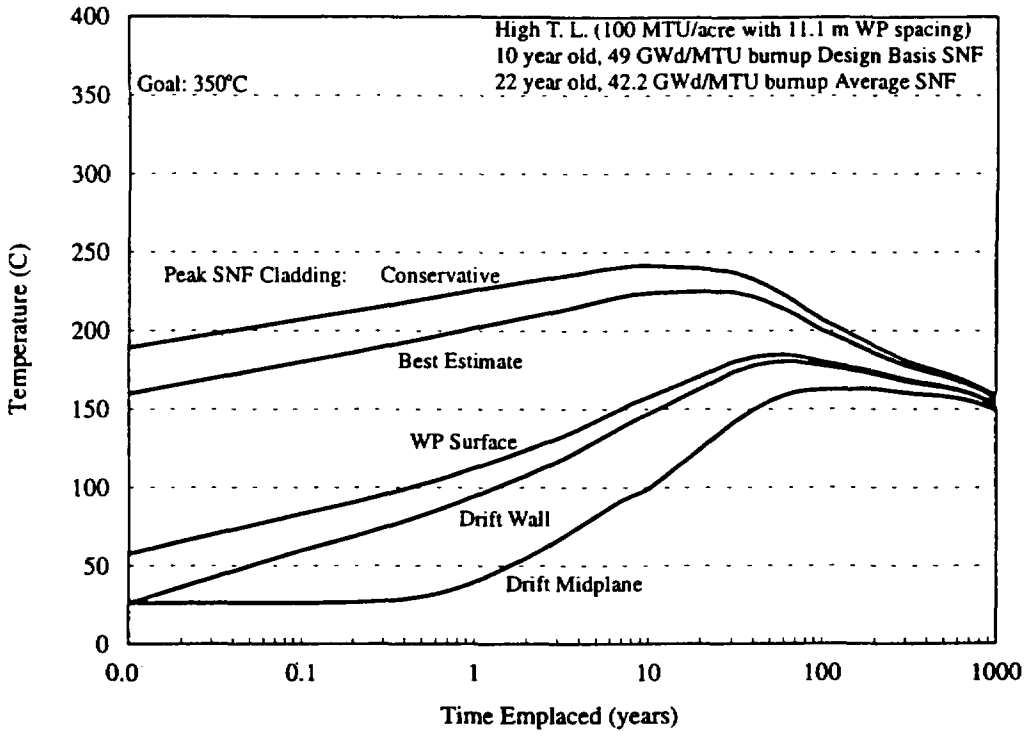


Figure 6.3-35. 24 BWR MPC, High Thermal Load (#1), MGDS DBF

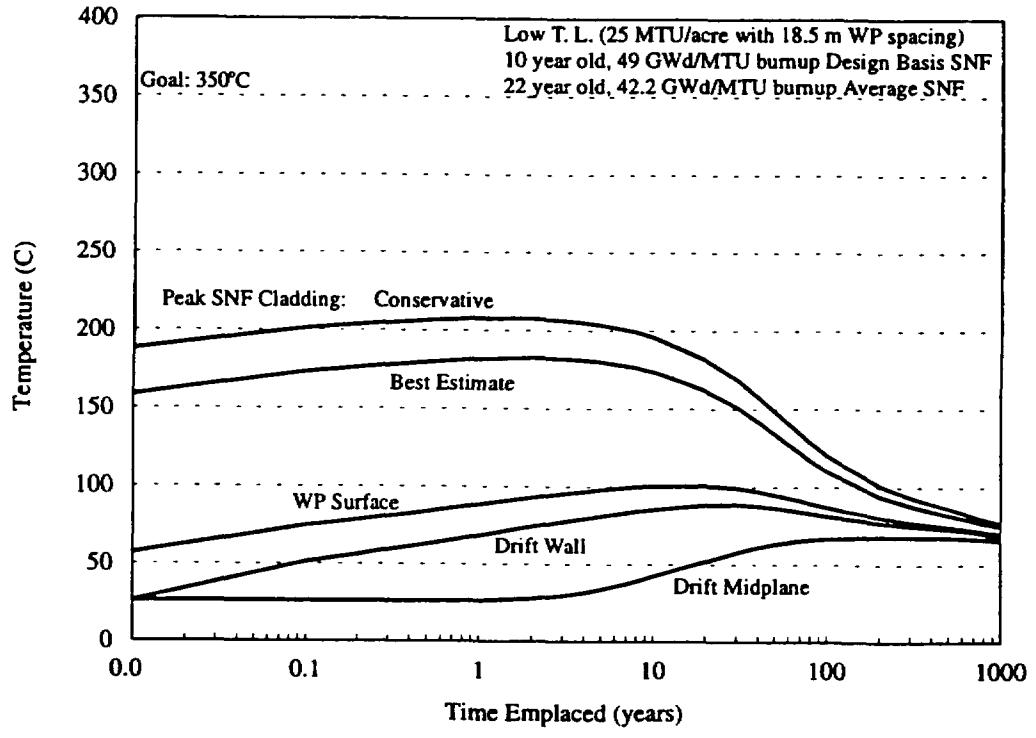


Figure 6.3-36. 24 BWR UCF, Low Thermal Load (#1), MGDS DBF

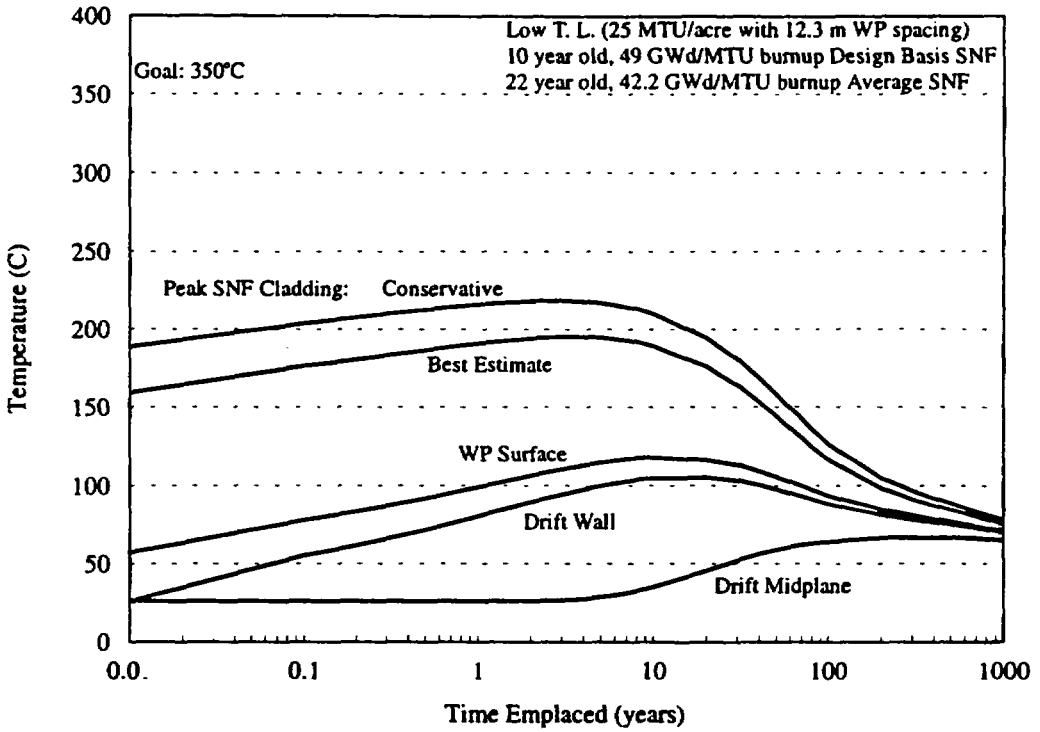


Figure 6.3-37. BWR MPC, Low Thermal Load (#2), MGDS DBF

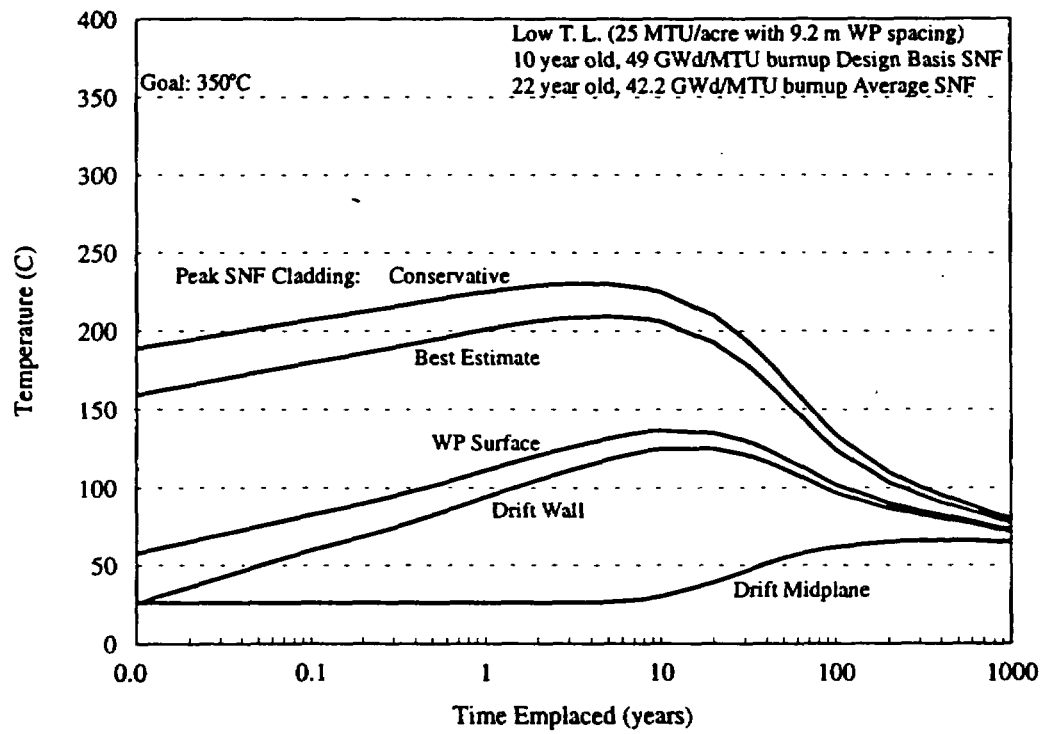


Figure 6.3-38. 24 BWR UCF, Low Thermal Load (#3), MGDS DBF

### 6.3.4 Structural Analysis

The WP must be shown to comply with all regulations and requirements that govern the containment of radionuclides. The regulations that the design must meet include 10 CFR 20, 10 CFR 60, and 40 CFR 191. These requirements state that the WP must remain intact as a unit for containing SNF and operational loads without loss of containment. Furthermore, it must be shown that the WP can survive design-basis accidents either without loss of containment or with a limited release of radionuclides.

The most damaging loads the WP must be able to endure are accident loads. Drawing from previous licensing work on transportation casks, the accidents analyzed were found to be drop and uncontrolled tip over or "slap down" accidents. Another potential accident condition which has been determined to be likely in the MGDS is the fall of a rock onto the WP. Therefore, the accident scenarios analyzed for the WPs are a WP 2m drop, slap down, and a starter tunnel rock fall. Design basis events are currently being determined and will be the subject of future work. To be conservative, the acceptance criteria will be to show that there is no breaching of the WP barriers, excluding the skirts (the extensions of the outer barrier cylinder used for handling purposes). Material failure in the outer barrier skirts is acceptable because the skirts are not part of the containment barrier. Plastic deformation of the barriers is also acceptable during these accidents provided that there is no rupture of the material. Four different WPs are analyzed for these accidents: 21 PWR UCF tube, 44 BWR UCF tube, 12 PWR UCF tube, and 24 BWR UCF tube designs. Throughout Section 6.3.4, these WPs will be referred to as the 21 PWR, 44 BWR, 12 PWR, and 24 BWR.

The material properties used in the calculations are given in Table 6.3-6. Material behavior is approximated in the model with elastic/plastic bilinear stress-strain curves for the materials. The calculations are performed with room temperature properties because A 516 properties at elevated temperatures were not available. Mechanical properties of Type 316L stainless steel and Alloy 825 have little temperature dependence for the temperatures of interest. ASTM A 516 carbon steel has decreasing strength but increasing ductility at high temperatures (below the material creep temperature). Ductile materials tend to absorb more energy due to impact loads. Therefore, this assumption has only a minor effect on the results.

#### 6.3.4.1 Waste Package 2-m Drop Accident Analysis

Prior to licensing, the WP must be shown to be capable of surviving certain accident conditions without resulting in a breach of radionuclide containment. One possibly damaging accident is a drop of the WP. The maximum height to which the WP is assumed to be lifted during transportation is 2 m (CRWMS M&O 1995n). Therefore, this height is selected for the WP drop analysis.

This hypothetical accident condition is a free drop of the WP from a height of 2 m onto a flat, essentially unyielding, horizontal surface. The horizontal surface cannot be perfectly unyielding because that would require a surface with infinite stiffness. Because such a surface cannot be modeled, these analyses use the next best option—an essentially unyielding surface which has a very high stiffness. The case analyzed is one in which the WP strikes the ground at an angle that puts the center of mass directly above the point of impact. These conditions cause the highest loads on the

WP outer barrier and therefore are expected to cause the most damage. The models described and the analysis results given in Section 6.3.4.1 are taken from *Finite-Element Analysis of Two Meter Drop of Uncanistered Fuel Waste Package Designs* (CRWMS M&O 1996h).

Table 6.3-6. Material Properties Table for Uncanistered Fuel Waste Package Models

| Material | Temp. | Yield Strength $S_y$ | Ultimate Tensile Strength $S_u$ | Elastic Modulus E | Poisson's Ratio υ | Percent Elongation |
|---|---|---|---|---|---|---|
| 316L | 20°C | 172 MPa[a] | 482 MPa[a] | 195 GPa[b] | 0.298[c] | 40[a] |
| A 516 Grade 55 | 20°C | 205 MPa[d] | 380 MPa[d] | 206 GPa[e] | 0.30[e] | 27[d] |
| Alloy 825 | 20°C | 338 MPa[f] | 662 MPa[f] | 206 GPa[f] | 0.42[f] | 45[f] |
| Rock* | - | - | - | 32.7 GPa[g] | 0.22[g] | - |

Table Notes:

* Stresses in the rock are not evaluated because the rock is assumed not to fail, so the only rock properties of importance are the elastic modulus and Poisson's ratio, which provide the rock with its stiffness. No plastic properties of the rock are included.

a. Holt, John M., Harold Mindlin, and C.Y. Ho 1992. (pp. 3-5)
b. ASME 1992. (Section II, Part D, Subpart 2, Table TM-1)
c. *Metals Handbook, Ninth Edition, Volume 3, Properties and Selection: Stainless Steels, Tool Materials and Special-Purpose Metals.* (p. 755)
d. ASTM A 516/A 516M 1990. (p. 321)
e. *Metals Handbook, Tenth Edition, Volume 1, Properties and Selection: Irons, Steels, and High-Performance Alloys.* (p. 374)
f. *INCO Alloys International* 1992. (p. 3)
g. YMP 1994a

### 6.3.4.1.1 21 PWR Uncanistered Fuel Tube Design

#### 6.3.4.1.1.1 Description of Finite-Element Model for WP 2-m Drop

The ANSYS 5.0A finite-element analysis code is used for the structural analysis of the WP 2-m drop accident scenario. Three-dimensional brick elements are used in modeling all parts of the WP. Some capabilities of the element used to perform this nonlinear transient dynamic analysis are plasticity, large deflection, and large strain.

The model developed for the 2-m drop analysis of the 21 PWR is a one-half symmetry, three-dimensional finite-element model, shown in Figure 6.3-39. The analysis incorporates the UCF tube basket assembly including structural angles, inner barrier, outer barrier, and SNF assembly weight. The weight of the aluminum plates is included in the model; however, no structural credit is taken for the aluminum plates. Material specifications of the tube basket assembly, inner barrier, and outer barrier are defined by their individual property tables. The tube basket assembly is given properties of 316L stainless steel, the inner barrier is given properties of Alloy 825, and the outer barrier is given properties of A 516.

The WP is symmetric about a plane that runs along the longitudinal axis, so only half of the WP is modeled, and symmetry boundary constraints are placed on the symmetry plane. This approach has been verified on a simple model which shows that stress distribution results obtained for both half and full models are identical in terms of normal and shear stress components. Stress plots are provided in Figures 6.5-52 and 6.5-53.

Taking advantage of the symmetry reduces the model size, allowing more detail in the half that is modeled. However, even with the half model, the element mesh must remain somewhat coarse to keep run times down and maintain manageability of the output files. Therefore, some other simplifications have been made to the model.

- The model is constructed as if the inner and outer barriers are fabricated as one piece. It is not yet known if the WP will be fabricated in this manner, but using this assumption prevents the need for contact elements between the inner and outer barriers. It is best to avoid the use of contact elements wherever possible to prevent convergence problems and to reduce the model size and run times. While the inner and outer barriers are treated as contiguous, there is an element border between the inner and outer barriers, and the appropriate material properties are used for each barrier.

- The basket assembly is extended along the WP length in order to fill in the 10 mm gap between the inner surface of the inner lids and the tubes. The tubes are also modeled as if the basket is a single piece of 316L stainless steel. These simplifications keep the finite-element model from including the complex geometries and discontinuities between the inner parts of the WP, which would have required the use of contact elements.

- Because of limited data in the literature for temperature dependent mechanical and physical properties, room temperature is used as a reference for all materials in the finite-element model. Mechanical properties of Type 316L stainless steel and Alloy 825 have little temperature dependence for the temperatures of interest. ASTM A 516 carbon steel has decreasing strength but increasing ductility at high temperatures (below the material creep temperature). Ductile materials tend to absorb more energy due to impact loads than brittle materials. Therefore, this assumption has only a minor effect on the results.

- The aluminum thermal shunt is not included in the finite-element model. However, its mass is included in the overall WP mass, making this approach conservative for the WP drop accident scenario.

- The SNF load has been calculated for the 21 PWR UCF tube design, and incorporated into the basket assembly mass. This has been accomplished by increasing the density of the 316L stainless steel in proportion to the mass for a constant volume of the basket assembly.

The simplifications made in this model are deemed reasonable because for conceptual design, overall system response is more important than the discrete calculation of stresses in the various radii and corners that a finer mesh allows. These discrete calculations will be performed at a later design stage.

The only force acting on the WP is its own mass times gravity. Maximum linear momentum transfer of the WP will occur along a vertical plane passing through its center of gravity, so the WP has been rotated 16.98° with respect to the vertical plane. This puts the center of mass directly above the contact point with the ground, causing the WP to be in an orientation that will result in maximum plastic deformation on the outer barrier skirt. The distance from the flat surface to the WP bottom edge is 2 m.

#### 6.3.4.1.1.2 Containment Barrier and Spent Fuel Assembly Basket Responses

As is described in the previous section, the drop considered is a corner drop with the WP rotated 16.98° from vertical. A corner drop can be separated into two individual drop events: initial impact and slap down. For WP impact angles near vertical, the initial impact dominates and the WP response resembles the condition of an end drop. For impact angles near horizontal, the slap down phase dominates and the assembly response resembles the condition of a side drop (SNL 1992a). A corner drop of 16.98° with respect to the vertical axis resembles the condition of an end drop and results in the largest deformation pattern on the barrier. Thus, the effect of second impact on the opposite end of the WP will not be critical when compared to the first impact. The slap down case is analyzed separately and the results are given in Section 6.3.4.2.

The skirt on the outer barrier behaves as an impact limiter during the WP 2-m corner-drop accident scenario. The linear momentum of the WP in the vertical direction results in maximum damage on the skirt in terms of elastic and plastic deformations. Figure 6.3-40 shows the principal stress distribution ($S_1$) on the WP and on the locally deformed region in the vicinity of the contact area with the flat surface.

An outer barrier breach can occur by ductile tearing as a result of excessive stress or strain. Sharp curvature bending of the impacted WP corner is the reason for very high stress magnitudes, which may result in ductile rupture. However, since the skirt functions as an impact limiter in this accident condition, failure is expected at the skirt location of the 21 PWR tube WP. Failure is acceptable in the skirt because a failure in this region will not result in a breach of the containment barrier. As can be observed in Figure 6.3-41, the effect of impact is not critical in any regions of the outer barrier other than the skirt.

The inner surface of the skirt makes a 90° angle with the WP outer lid at the location where the skirt is extended from the container. This sharp corner could be eliminated by introducing a corner radius during the manufacturing process. This might slightly reduce the excessive deformation of the skirt by increasing its stiffness. However, the effect of a corner radius would still not be able to prevent the skirt from deforming plastically because the dynamic loading on the skirt is very high.

The transient simulation of dynamic loading during the drop was terminated after the first impact since the second impact was previously determined to be less critical than the first. Therefore, the analysis was performed to determine the maximum stress due to the first impact. It should also be noted that the time step of the finite-element analysis from which the results are taken was selected to include the maximum deformation pattern on the containment barrier.

The maximum stress and strain magnitudes were obtained in the vicinity of the outer barrier skirt where the impact causes local ductile rupture. The maximum principal stress magnitude on the WP is 1230 MPa, see Figure 6.3-40. When the ultimate tensile strength of the outer barrier (380 MPa) is compared to the first principal stress value (1230 MPa), it can be concluded that there is a localized material failure around the region of impact in the skirt. Figure 6.3-41 shows that there is no material failure in any part of the outer barrier other than in the skirt since the maximum first principal stress (355 MPa) is less than the ultimate tensile strength of the outer barrier (380 MPa) for this region.

In the basket assembly of the finite-element model, the stress does not exceed 37.6 MPa, see Figure 6.3-42. This is below the yield strength of the basket assembly material (172 MPa), so there is no plastic deformation in the basket due to a WP 2-m corner drop accident.

It is concluded that the WP 2-m drop accident will cause ductile rupture of the skirt. However, there will be no failure in any critical regions of the WP because the stress magnitudes are below the ultimate tensile strength in the inner and outer barriers, and below the yield strength in the basket assembly.

#### 6.3.4.1.2 44 BWR Uncanistered Fuel Tube Design

##### 6.3.4.1.2.1 Description of Finite-Element Model for WP 2-m Drop

Because the mass and area moment of inertia characteristics for the 44 BWR are similar to those for the 21 PWR, one finite-element model has been considered to represent both WP concepts. Qualitative comparisons are made in Section 6.3.4.1.2.2.

##### 6.3.4.1.2.2 Containment Barrier and Spent Fuel Assembly Basket Responses

The mass of the 44 BWR is slightly less (see Table 6.1-4) than that of the 21 PWR. Therefore, deformation patterns and stress distributions obtained for the 21 PWR are considered to be limiting. Thus, the worst case containment barrier stresses for the large UCF WP are presented in Section 6.3.4.1.1.2.

Loads on the tubes of the basket assembly during a WP 2-m drop will be approximately the same for the 44 BWR as for the 21 PWR. However, the 44 BWR basket assembly has a larger number of tubes that have a smaller side length than the tubes for the 21 PWR, but also have thinner walls. Smaller side length increases tube strength while the thinner wall reduces tube strength. The overall effect is that the strength of an individual 44 BWR tube is slightly less than the strength of an individual 21 PWR tube. However, the load is distributed on approximately twice as many tubes

in the 44 BWR as in the 21 PWR. Therefore, the basket of the 44 BWR will be able to take more load than the basket of the 21 PWR. For this reason, the basket stresses of the 21 PWR are considered limiting for the large UCF Tube Designs, see Section 6.3.4.1.1.2.

#### 6.3.4.1.3 12 PWR Uncanistered Fuel Tube Design

##### 6.3.4.1.3.1 Description of Finite-Element Model for Waste Package 2-m Drop

The model developed for the 2-m drop analysis of the 12 PWR is a one-half symmetry three-dimensional finite-element model, shown in Figure 6.3-43. The analysis incorporates the UCF tube basket assembly, inner barrier, outer barrier, and SNF assembly weight as they were previously modeled for 21 PWR configuration. However, there are a few differences in the geometry of the finite-element mesh. The containment barrier diameters are smaller, and there are fewer fuel assembly tubes in the basket assembly.

Like the 21 PWR, the 12 PWR is symmetric about a plane that runs along the longitudinal axis, so only half of the WP is modeled, and symmetry boundary constraints are placed on the symmetry plane. Taking advantage of the symmetry reduces the model size, allowing more detail in the half that is modeled. However, even with the half model, the element mesh must remain somewhat coarse to keep run times down and maintain manageability of the output files. The number of elements used for mesh generation of the 12 PWR is less than the number of elements generated for the 21 PWR configuration due to the decreased number of fuel assembly tubes in the basket assembly structure. Therefore, the same simplifications and assumptions made for the 21 PWR model, see Section 6.3.4.1.1.1, have been made to this model.

Maximum linear momentum transfer of the WP will occur along a vertical plane passing through its center of gravity, so the WP has been rotated 13.67° with respect to the vertical plane. This puts the center of mass directly above the contact point with the ground, causing the WP to be in an orientation that will result in maximum plastic deformation of the outer barrier skirt. The distance from the flat surface to the WP bottom edge is 2 m.

##### 6.3.4.1.3.2 Containment Barrier and Spent Fuel Assembly Basket Responses

As is described in the previous section, the drop considered is a corner drop with the WP rotated 13.67° from vertical. A corner drop can be comprised of two separate drop events: initial impact and slap down. For WP impact angles near vertical, the initial impact dominates and the WP response resembles the condition of an end drop. For impact angles near horizontal, the slap down phase dominates and the assembly response resembles the condition of a side drop (SNL 1992a). A corner drop of 13.67° with respect to the vertical axis resembles the condition of an end drop and results in the largest deformation pattern on the barrier. Thus the effect of second impact on the opposite end of the WP will not be critical when compared to the first impact. The slap down case is analyzed separately and the results are given in Section 6.3.4.2.

The skirt on the outer barrier behaves as an impact limiter during the WP 2-m corner drop accident scenario. The linear momentum of the WP in the vertical direction results in maximum damage on the skirt in terms of elastic and plastic deformations. Figure 6.3-44 shows the principal stress distribution ($S_1$) on the WP and on the locally deformed region in the vicinity of the contact area with the flat surface.

An outer barrier breach can occur by ductile tearing as a result of excessive stress or strain. Sharp curvature bending of the impacted WP corner is the reason for very high stress magnitudes, which may result in ductile rupture. However, since the skirt functions as an impact limiter in this accident condition, failure is expected at the skirt location of the 12 PWR Tube WP. Failure is acceptable in the skirt because a failure in this region will not result in a breach of the containment barrier. As can be seen in Figure 6.3-45, the effect of impact is not critical in any regions of the outer barrier other than in the skirt.

The transient simulation of dynamic loading during the drop was terminated after the first impact since the second impact was previously determined to be less critical than the first. It should also be noted that the time step of the finite-element analysis from which the results are taken was selected to include the maximum deformation pattern on the containment barrier.

The mass of the 12 PWR is nearly 15 metric tons less than the mass of the 21 PWR configuration, see Table 6.1-4. Considerable differences in the mass and geometry cause different stress magnitudes and distribution after the impact of the 12 PWR on the flat surface. The maximum stress at the impact region is 1,000 MPa, see Figure 6.3-44. This magnitude of stress causes ductile rupture of the material in the skirt. The mechanism of this failure and its location raise a discussion similar to that made for the 21 PWR.

When the ultimate tensile strength of the outer barrier (380 MPa) is compared to the first principal stress value (1,000 MPa), it can be concluded that there is a localized material failure around the region of impact in the skirt (Figure 6.3-44). However, there is no material failure in any part of the outer barrier other than the skirt since the maximum first principal stress (337 MPa) is less than the ultimate tensile strength of the outer barrier material (380 MPa), see Figure 6.3-45.

In the basket assembly of the finite-element model, the stress does not exceed 33.1 MPa, see Figure 6.3-46. This is below the yield strength of the basket assembly material (172 MPa), so there is no plastic deformation in the basket due to a WP 2-m corner drop accident.

It is concluded that the WP 2-m drop accident will cause ductile rupture of the skirt. However, there will be no failure in any critical regions of the WP because the stress magnitudes are below the ultimate tensile strength in the inner and outer barriers, and below the yield strength in the basket assembly.

#### 6.3.4.1.4 24 BWR Uncanistered Fuel Tube Design

##### 6.3.4.1.4.1 Description of Finite-Element Model for Waste Package 2-m Drop

Because the mass and area moment of inertia characteristics for the 12 PWR are similar to those for the 24 BWR, one finite-element model has been considered to represent both WP concepts. Qualitative comparisons are made in Section 6.3.4.1.4.2.

##### 6.3.4.1.4.2 Containment Barrier and Spent Fuel Assembly Basket Responses

The mass of the 24 BWR is slightly less (see Table 6.1-4) than that of the 12 PWR. Therefore, deformation patterns and stress distributions obtained for the 12 PWR are considered to be limiting. Thus, the worst case containment barrier stresses for the small UCF WP are presented in Section 6.3.4.1.3.2.

Loads on the tubes of the basket assembly during a WP 2-m drop will be approximately the same for the 24 BWR as for the 12 PWR. However, the 24 BWR basket assembly has a larger number of tubes that have a smaller side length than the tubes for the 12 PWR, but also have thinner walls. Smaller side length increases tube strength while the thinner wall reduces the tube strength. The overall effect is that the strength of an individual 24 BWR tube is slightly less than the strength of an individual 12 PWR tube. However, the load is distributed on approximately twice as many tubes in the 24 BWR as in the 12 PWR. Therefore, the basket of the 24 BWR will be able to take more load than the basket of the 12 PWR. For this reason, the basket stresses of the 12 PWR are considered limiting for the large UCF Tube Designs, see Section 6.3.4.1.3.2.

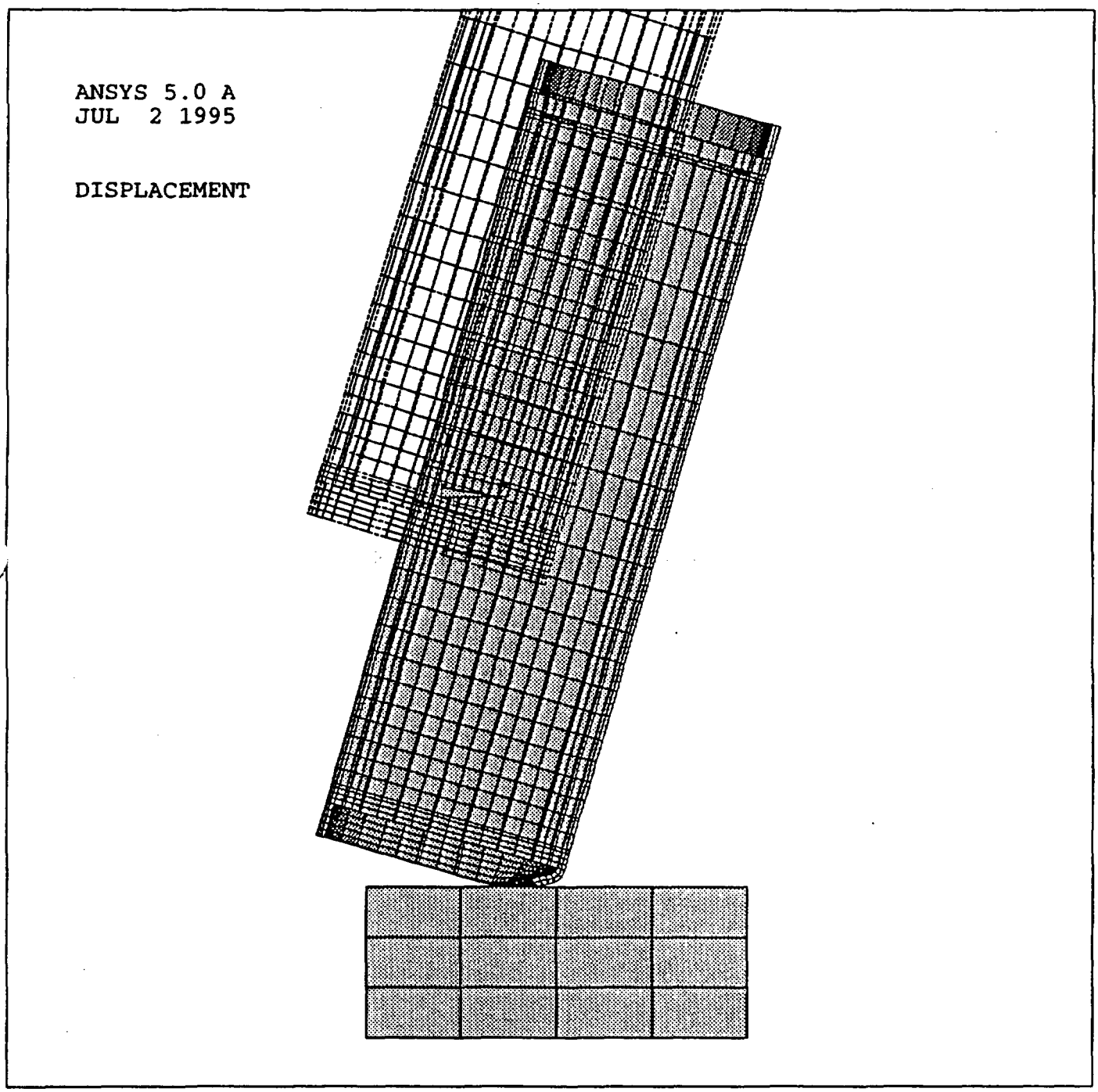


Figure 6.3-39. 21 PWR UCF Tube Design WP 2-m Drop Model

INTENTIONALLY LEFT BLANK

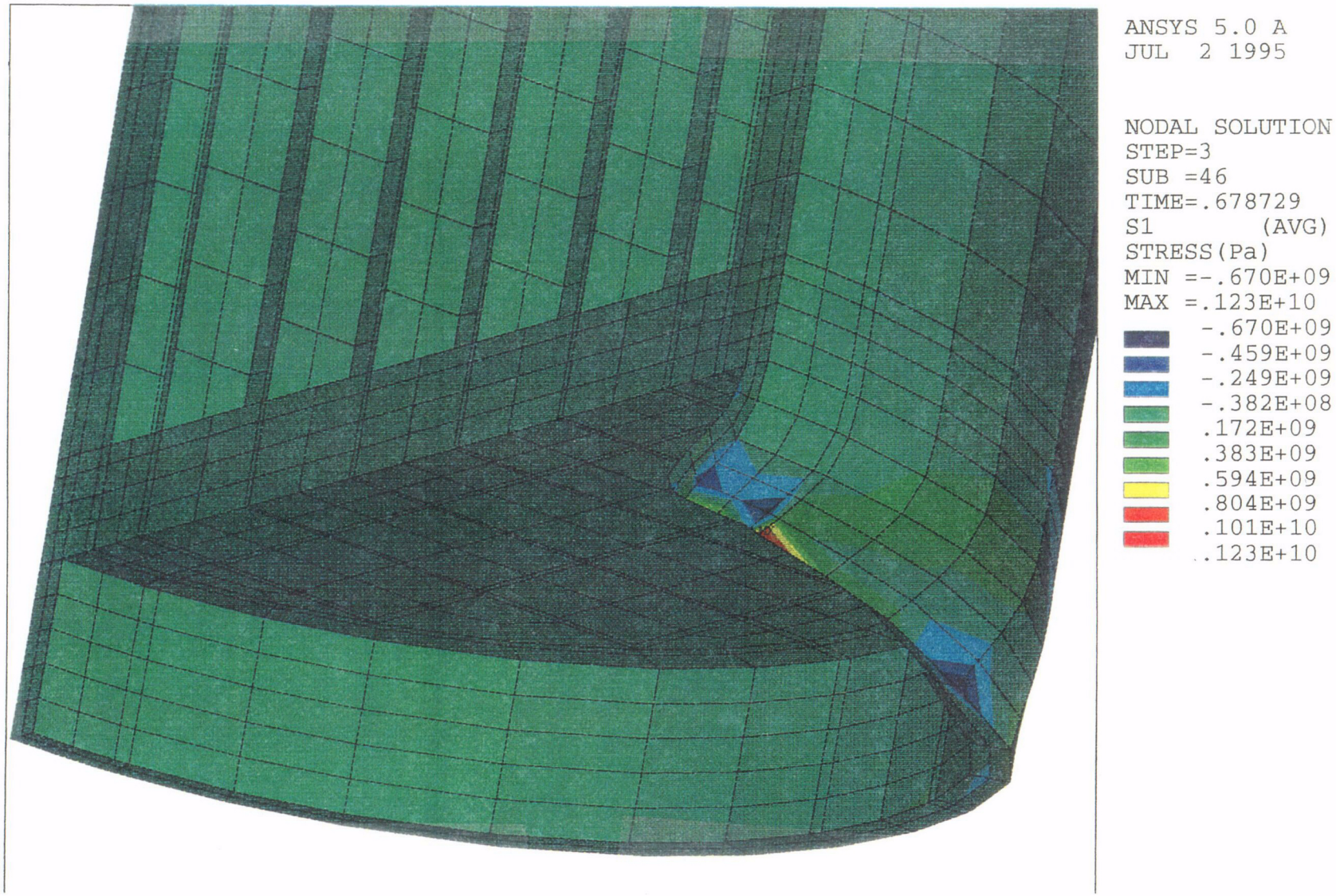


Figure 6.3-40. 21 PWR UCF Tube Design WP 2-m Drop Stress Contour

C08

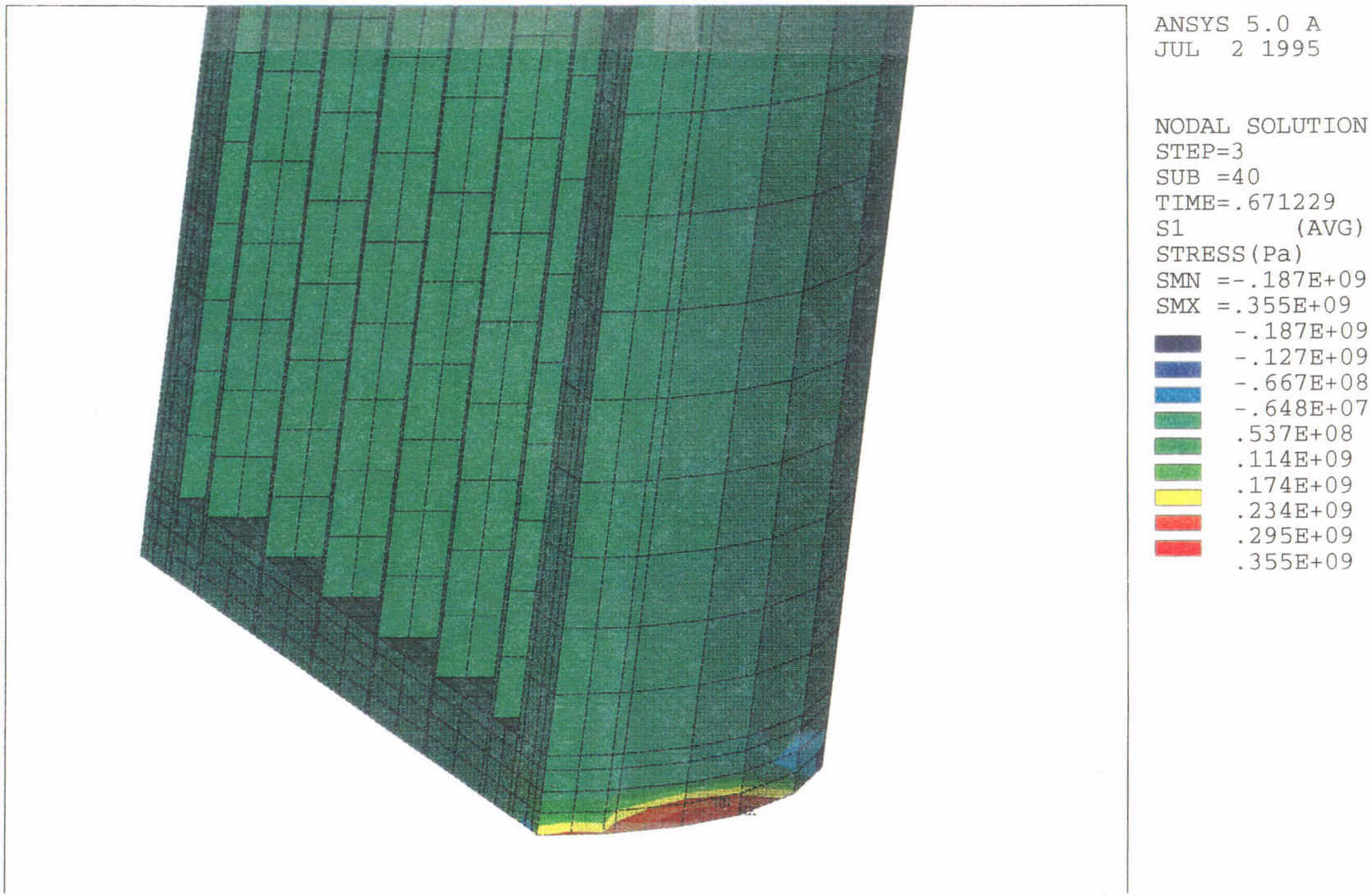


Figure 6.3-41. 21 PWR UCF Tube Design WP 2-m Drop Stress Contour (Without Skirt)

C09

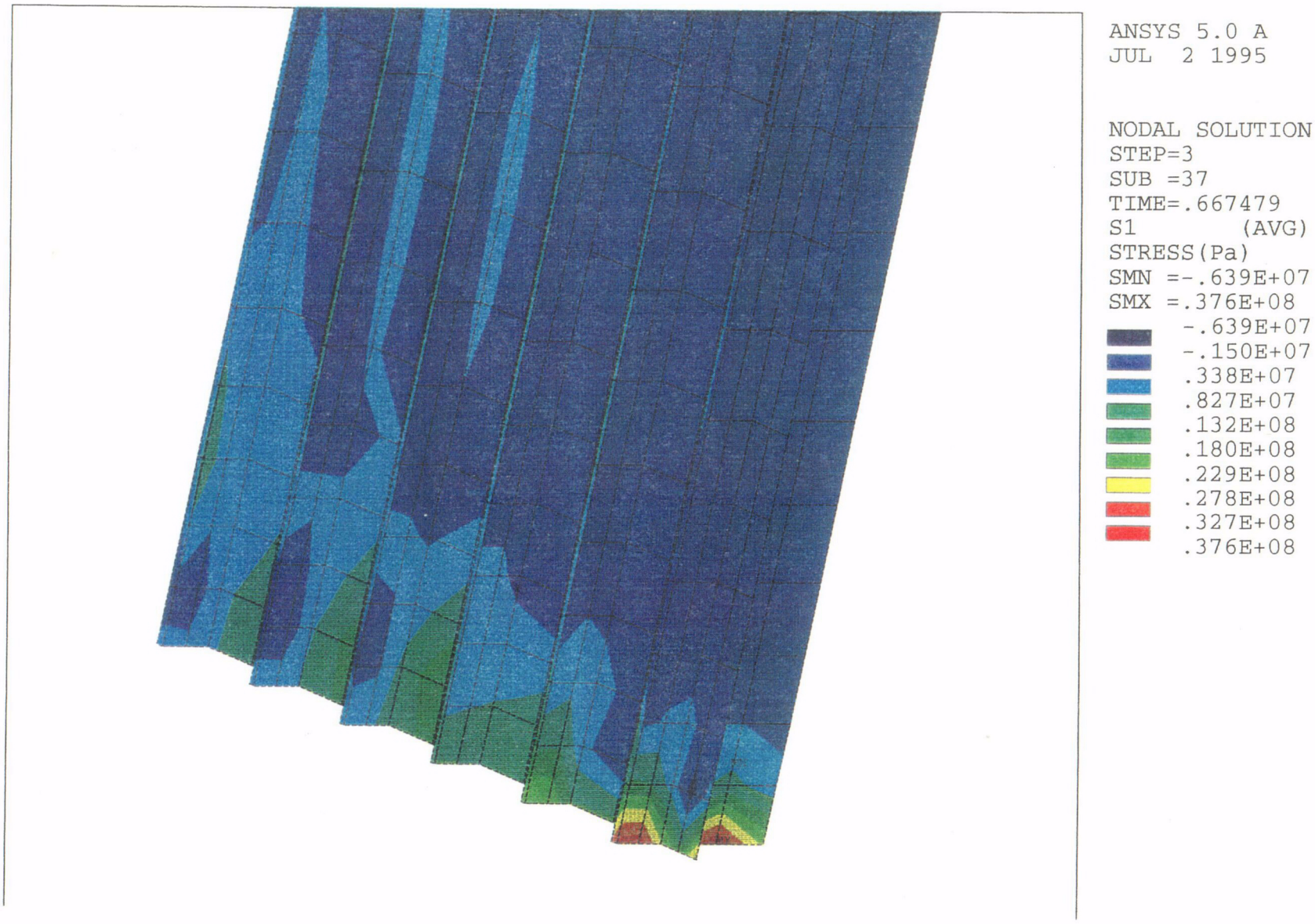


Figure 6.3-42. 21 PWR UCF Tube Design WP 2-m Drop Stress Contour (Basket Assembly)

C10

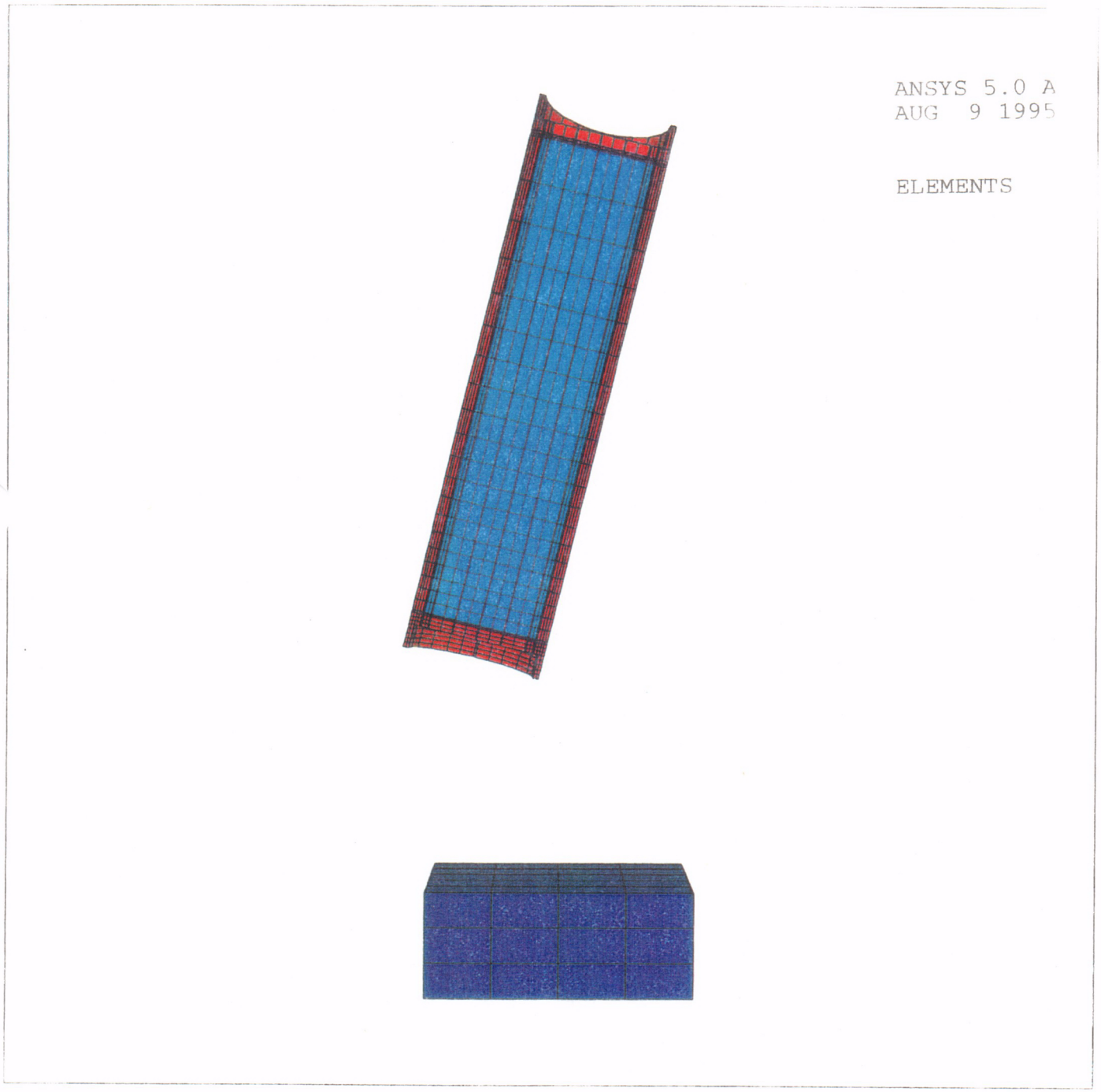


C11

Figure 6.3-43. 12 PWR UCF Tube Design WP 2-m Drop Model

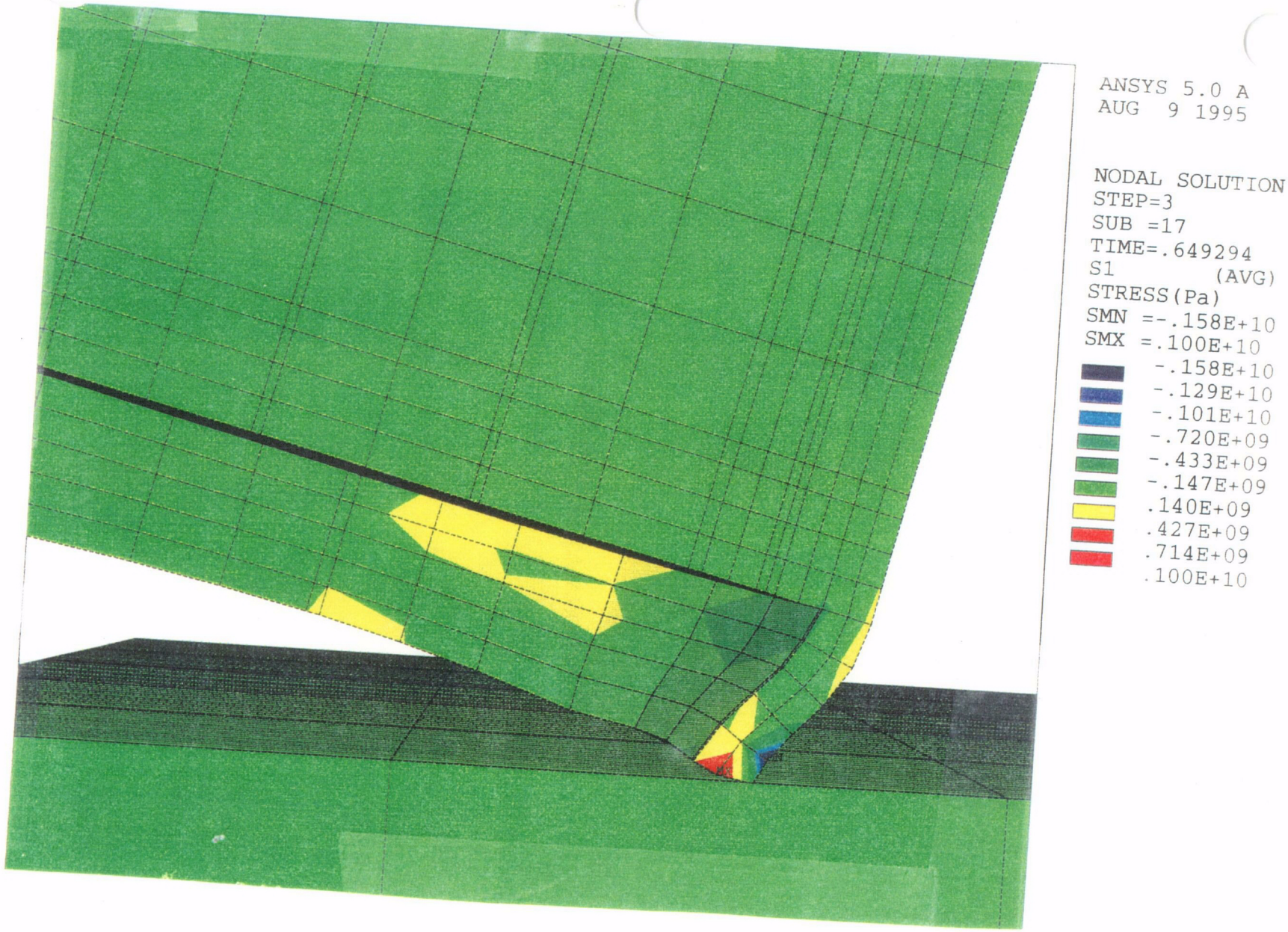


Figure 6.3-44. 12 PWR UCF Tube Design WP 2-m Drop Stress Contour

C12


C13

Figure 6.3-45. 12 PWR UCF Tube Design WP 2-m Drop Stress Contour (Without Skirt)

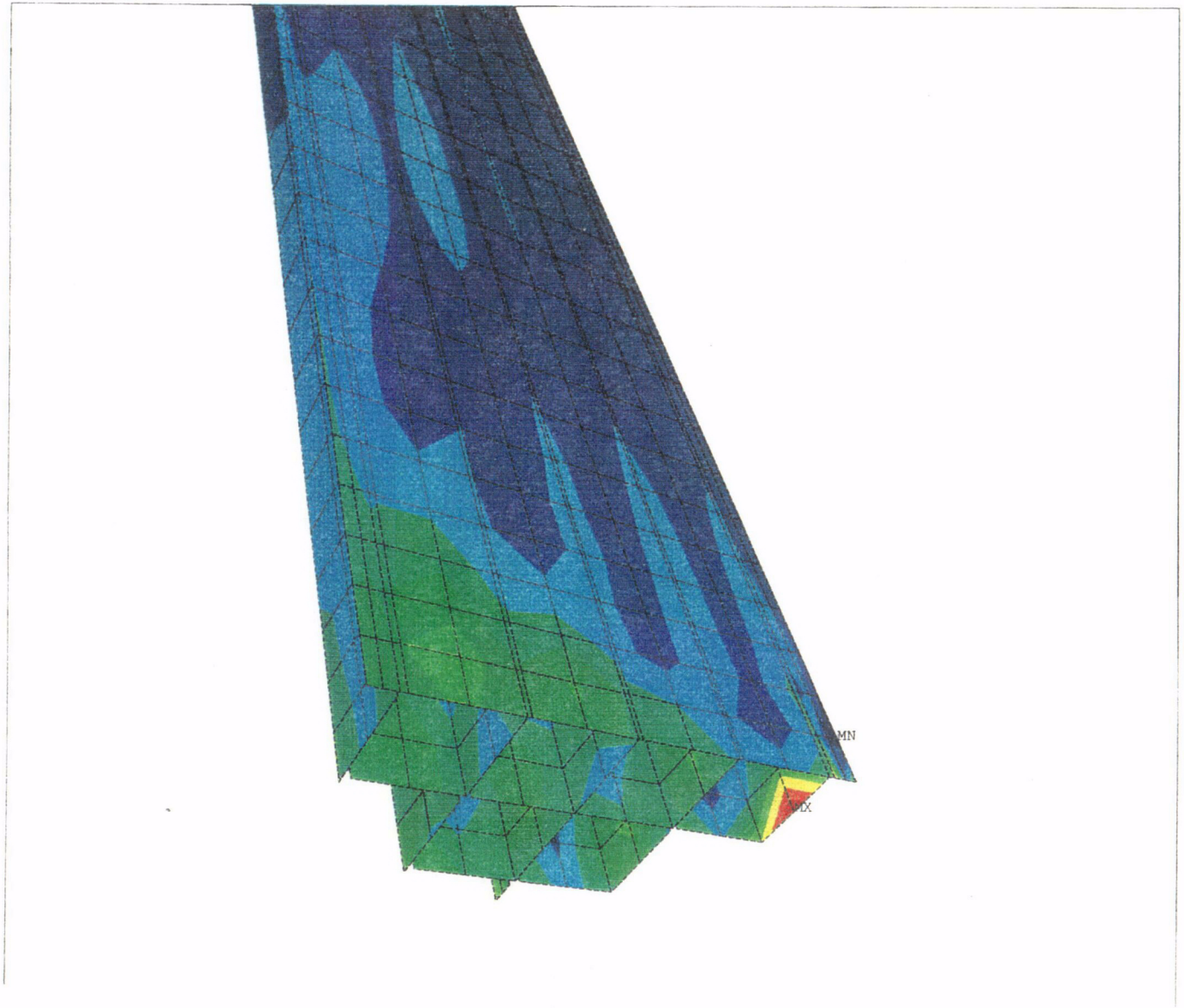


C14

Figure 6.3-46. 12 PWR UCF Tube Design WP 2-m Drop Stress Contour (Basket Assembly)